AD-A050 132 ILLINOIS UNIV AT URBANA-CHAMPAIGN ELECTROMAGNETICS LAB F/G 20/14
EFFICIENT COMPUTATION OF RADIATION PATTERNS AND CONTOUR BEAM SY--ETC(U)
SEP 77 R MITTRA AFOSR-77-3375
UNCLASSIFIED UIEM-77-18 AFOSR-TR-78-0034 NL

| OF |
AD
A050 132

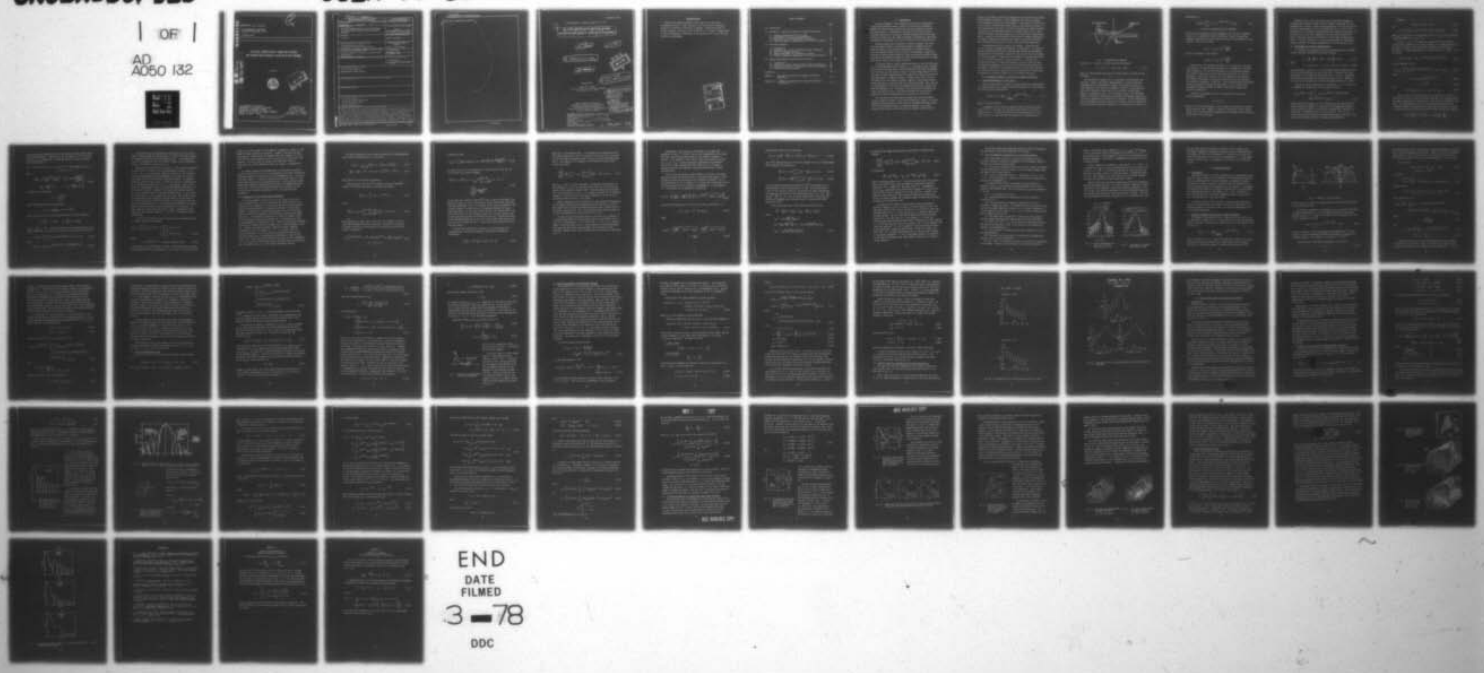

END
DATE
FILMED
3-78
DDC

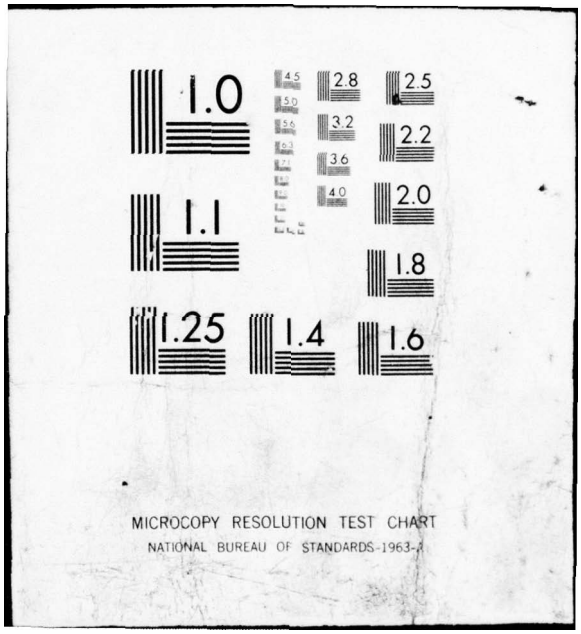
1.0
1.1
1.25
1.4
1.6
1.8
2.0
2.2
2.5
2.8
3.2
3.6
4.0
4.5
5.0
5.6
6.3
7.1
8.0
9.0
MICROCOPY RESOLUTION TEST CHART
NATIONAL BUREAU OF STANDARDS-1963-A

AFOSR-TR- 78-0034

ELECTROMAGNETICS LABORATORY
SCIENTIFIC REPORT NO. 77-18

September 1977

EFFICIENT COMPUTATION OF RADIATION PATTERNS AND CONTOUR BEAM SYNTHESIS USING REFLECTOR ANTENNAS

R. Mittra

ELECTROMAGNETICS LABORATORY
DEPARTMENT OF ELECTRICAL ENGINEERING
ENGINEERING EXPERIMENT STATION
UNIVERSITY OF ILLINOIS AT URBANA-CHAMPAIGN
URBANA, ILLINOIS 61801

Supported by
Grant No. 77-3375
Air Force Office
of Scientific Research
Washington, D.C. 20332

REPORT DOCUMENTATION PAGE

READ INSTRUCTIONS BEFORE COMPLETING FORM

1. REPORT NUMBER: AFOSR-TR-78-0034	2. GOVT ACCESSION NO.
3. RECIPIENT'S CATALOG NUMBER	
4. TITLE (and Subtitle): EFFICIENT COMPUTATION OF RADIATION PATTERNS AND CONTOUR BEAM SYNTHESIS USING REFLECTOR ANTENNAS	5. TYPE OF REPORT & PERIOD COVERED: Interim
	6. PERFORMING ORG. REPORT NUMBER: EM 77-18, UILU-ENG-77-2261
7. AUTHOR(s): R. Mittra	8. CONTRACT OR GRANT NUMBER(s): AFOSR 77-3375
9. PERFORMING ORGANIZATION NAME AND ADDRESS: Electromagnetics Laboratory, Department of Electrical Engineering, University of Illinois, Urbana, Illinois 61801	10. PROGRAM ELEMENT, PROJECT, TASK AREA & WORK UNIT NUMBERS: 61102F; Project, Task 2305-B2
11. CONTROLLING OFFICE NAME AND ADDRESS: Air Force Office of Scientific Research (NE), Building 410, Bolling AFB, D.C. 20332	12. REPORT DATE: September 1977
	13. NUMBER OF PAGES: 57
14. MONITORING AGENCY NAME & ADDRESS (if different from Controlling Office)	15. SECURITY CLASS. (of this report): Unclassified
	15a. DECLASSIFICATION DOWNGRADING SCHEDULE

16. DISTRIBUTION STATEMENT (of this Report)

Distribution Unlimited.

Approved for Public Release

17. DISTRIBUTION STATEMENT (of the abstract entered in Block 20, if different from Report)

18. SUPPLEMENTARY NOTES

19. KEY WORDS (Continue on reverse side if necessary and identify by block number)

Reflector Antennas
Secondary Pattern Computation
Series Expansion Method
Offset Reflectors
Contour Beam Synthesis

20. ABSTRACT (Continue on reverse side if necessary and identify by block number)

In this report, we discuss two important aspects of reflector antennas, viz., secondary pattern computation of symmetric and offset reflectors and the problem of synthesizing contour beams using reflector antennas. A new technique is described for computing the radiation pattern from the knowledge of the surface current of the reflector, or the primary pattern of the feed. Numerical results illustrating the efficiency of the method are given. Finally, two methods for addressing the problem of synthesizing contour beams are presented. One of these is basically an analytical technique and the other is based on a numerical (OVER)

Block 20. optimization procedure.

UILU-ENG-77-2261

Electromagnetics Laboratory Report No. 77-18

EFFICIENT COMPUTATION OF RADIATION PATTERNS AND CONTOUR BEAM SYNTHESIS USING REFLECTOR ANTENNAS

by

R. Mittra

58P.

Interim Scientific Report

September 1977

UIEM-77-18,
UILU-ENG-77-2261

Supported by

Grant No. 77-3375
Air Force Office of Scientific Research
Washington, D.C. 20332

AFOSR-77-3375

2305

B2

AFOSR

TR-78-0034

Electromagnetics Laboratory
Department of Electrical Engineering
Engineering Experiment Station
University of Illinois at Urbana-Champaign
Urbana, Illinois 61801

408 102 JOB

ACKNOWLEDGEMENT

Much of the research reported in this work was carried out in collaboration with Dr. Victor Galindo of the Jet Propulsion Laboratory, California Institute of Technology in Pasadena, to whom the author is greatly indebted. Discussions with Professor S. W. Lee and Y. Rahmat-Samii of the Electromagnetics Laboratory of the University of Illinois are also gratefully acknowledged.

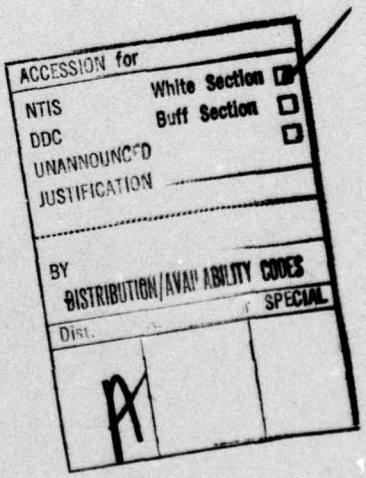

TABLE OF CONTENTS

		Page
1.0	Introduction	1
2.0	Evaluation of Radiation Integral for Symmetric Reflectors	2
2.1	Integral Representation of Far Field	2
2.2	Development of the Series Representation	5
2.3	Evaluation of (2.12) Using Jacobi Polynomials	9
2.4	Steps for Numerical Computations and Illustrative Results	16
3.0	The Offset Reflector	18
3.1	Introduction	18
3.2	Radiation Integral for the Offset Parabolic Reflector	18
3.3	Choice of Optimum Scan Plane	22
3.4	Series Development of the Radiation Integral	26
3.5	Steps for Numerical Computation and Illustrative Results	29
4.0	Contour Beam Synthesis Using Reflector Antennas	31
4.1	Introduction	31
4.2	Synthesis of Cluster Feeds to Reduce Pattern Distortion	32
4.3	Illustrative Results of Cluster and Contour Beam Synthesis	40
4.4	Gradient Optimization Method	45
References		49
Appendix I.	Beam Deviation Factors for Symmetric Reflectors (Parabolic)	50
Appendix II.	A Method for Computing the "Equivalent Aperture" Distribution	51

1.0 Introduction

Increasing demands on the performance of satellite communication antennas have generated recent interest in efficient and systematic methods for analyzing and synthesizing reflector antennas and associated feed systems. A comprehensive discussion of a diverse array of available techniques for analyzing reflector antennas has recently been published by Rusch [1]; the reader interested in developing a good broad background on the subject will do well to refer to this excellent work.

Scanning through the literature on reflector antennas, one finds that most workers prefer to use methods based on integration of the induced currents on the reflector to compute its secondary pattern. Also, the induced current on the surface of the reflector is typically derived via the well-known "physical optics" approximation which has been verified to be extremely accurate for predicting the pattern over a rather wide angular range in the forward direction.

In contrast, the ray optical methods are known to run into difficulty [2] in the neighborhood of the caustic, i.e., the beam maximum, although they work well at wide angles. Hybrid techniques that employ ray methods as a first step for deriving the fields in the projected aperture of the reflector and then integrating over this aperture to derive the far field have been used by a number of workers. However, they suffer from the shortcoming that the secondary patterns computed in this manner rapidly become inaccurate as one moves away from the beam maximum. Thus, the use of this approach is limited to the computation of the main beam and the near-end sidelobes only. Furthermore, the polarization information derived from either the ray or the hybrid approach can contain errors beyond the tolerance requirements on the accuracy of the results.

For the reasons outlined above, we choose to follow the induced current integration method in this work and describe in detail a recently developed series approach [3] that allows an extremely efficient evaluation of the radiation integral of reflector antennas. The series approach differs both in spirit as well as in detail from the various

numerical algorithms conventionally employed for increasing the efficiency of the numerical procedures [1] for evaluating the radiation integral. The development of the series representation is motivated by the fact that in the course of synthesizing contour beams, a topic which we discuss in the latter part of this paper, one finds it necessary to perform accurate computation of the secondary pattern of reflector antennas for a large number of laterally displaced feeds and over a wide range of observation angles. The series representation of the radiation integral developed in this paper allows one to accomplish this task in a much more efficient manner than would be possible via any of the conventional approaches.

The organization of this paper is as follows. In Section 2 we discuss the case of symmetrical reflectors in some detail. In Section 3 we deal with the offset reflector and show that certain transformations incorporated in the radiation integral for this case allow one to convert it into a form which is identical to the symmetric case, thus preserving all of the useful properties of the series form. In Section 4 we discuss the problem of contour beam synthesis using a cluster of feeds. We develop two approaches for deriving the excitation coefficients for the feeds, one based on an approximation method, and the other requiring the solution of a matrix equation that can be inverted in a closed form. A comparison of these two methods is also included in Section 4.

2.0 Evaluation of Radiation Integral for Symmetric Reflectors

2.1 Integral Representation of Far Field

The far field radiation integral (suitably normalized) representing the field produced by the induced current distribution $\bar{J}$ on the surface of the reflector can be expressed as

$$\bar{E}(\theta,\phi) = (\bar{\bar{I}} - \hat{R}_0\hat{R}_0) \cdot \iint_{SURFACE} \bar{J} e^{-jk(\rho' - \bar{\rho}\cdot\hat{R}_0)}\, ds, \qquad (2.1)$$

where $\bar{\bar{I}}$ = the unit dyadic.

The geometry of the reflector antenna system including the feed is shown in Fig. 1. We point out that the optical phase of $\bar{J}$ has been factored out in (2.1) where this phase is defined relative to an ideal phase center at $\bar{\varepsilon}$, which defines the location of the displaced feed

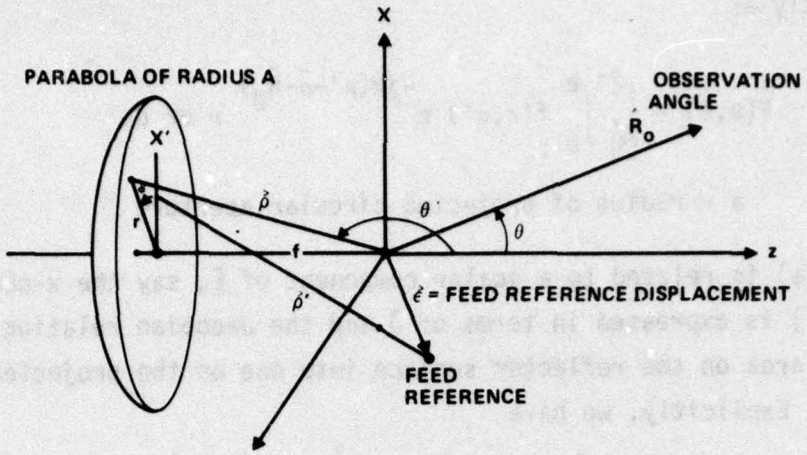

Fig. 1. Feed-reflector geometry.

(see Fig. 1). From Fig. 1 we also have the relationship

$$\bar{\rho}' = \bar{\rho} - \bar{\epsilon} = \bar{\rho} - (\hat{x}\epsilon_x + \hat{y}\epsilon_y + \hat{z}\epsilon_z) \quad , \tag{2.2}$$

where $\bar{\rho}$ is the distance from the origin (focal point) to a point on the reflector.

We note that the integral (2.1) is defined on the surface of the reflector. Often a ray-optical "approximation" is used to derive an alternate form for the radiation integral which requires the Fourier transformation of the electric and magnetic fields on a projected aperture of the reflector, rather than on the reflector surface itself. However, as mentioned earlier, this introduces errors in the secondary pattern calculation at observation angles away from the main beam direction and is therefore not suitable for our purpose. We can, nevertheless, derive a mathematically exact form of (2.1) which is also an integration over the projected aperture coordinates. For instance, we can write (2.1)

equivalently as

$$F(\theta,\phi) = \int_0^{2\pi}\int_0^{a} f(r,\phi')\, e^{-jk(\rho'-\bar{\rho}\cdot\hat{R}_0)}\, r\, dr\, d\phi' \qquad (2.3)$$

a = radius of projected circular aperture

where $F(\theta,\phi)$ is related to a scalar component of $\bar{E}$, say the x-component, and $f(r,\phi')$ is expressed in terms of $\bar{J}$ and the Jacobian relating the elemental area on the reflector surface into one on the projected circular aperture. Explicitly, we have

$$f(r,\phi') = J_x(r,\phi')\sqrt{1 + \left(\frac{dz}{dr}\right)^2} \quad , \qquad (2.4)$$

and for a parabola of focal length f,

$$f(r,\phi') = J_x(r,\phi')\sqrt{1 + \left(\frac{r}{2f}\right)^2} \quad .$$

The function f is sometimes referred to as the "equivalent aperture" distribution. It should be realized that this is somewhat of a misnomer since, physically, f is not the distribution on the projected aperture (in contrast to the one that can be derived approximately via the ray technique). Since (2.3) is exact, if f were indeed the true aperture distribution, the kernel of (2.3) would have had the Fourier transform form which, at the moment, it does not. One of the principal contributions of this work would be to show that the kernel in (2.3) can still be expressed in terms of a series of Fourier transforms of appropriate functions related to f.

Typically, the induced current $\bar{J}$ is derived from the physical optics approximation

$$\bar{J} = 2\hat{n} \times \bar{H}_i$$

where $\bar{H}_i$ is the primary magnetic field incident on the reflector surface due to the given feed. However, if desired, the physical optics approximation for $\bar{J}$ can be refined by augmenting it with fringe currents existing at the edges of the reflector.

Returning now to (2.3), we note that the conventional approach to evaluating the radiation integral entails repeated computation of this two-dimensional integral on the "equivalent aperture" for each observation direction which themselves form a two-dimensional grid. Even if some timesaving can be achieved by employing efficient numerical algorithms for evaluating (2.3), the total computation time can become prohibitively large if accurate results are desired over a wide range of observation angles. This fact motivates us to seek alternate means for handling the radiation integral in a manner elaborated on in the following section.

2.2 Development of the Series Representation

As a preamble to developing the series representation, we introduce certain notations, approximations and new variables:

$$\rho' = \rho\left\{1 - \left(\frac{\varepsilon_x}{\rho} u' + \frac{\varepsilon_y}{\rho} v' + \frac{\varepsilon_z}{\rho} w'\right)\right\} + O(\varepsilon^2) \quad , \tag{2.5a}$$

where

$$u' = \sin\theta' \cos\phi'; \; v' = \sin\theta' \sin\phi'; \; w' = \cos\theta' \tag{2.5b}$$

and the direction cosines u, v, w for the observation variables are likewise defined by removing the primes from (2.5b). Typically, for small displacement of the feed, the second-order term in (2.5a) is negligible and we make the approximation here that this term is small. However, it is only a trivial extension to include the higher-order term in (2.5a).

Scaling the radial coordinate r by introducing r = as, a = D/2, and D = diameter of the reflector, one may rewrite (2.3) as

$$F(u,v)\, e^{+jk2f} = a^2 \int_0^{2\pi} \int_0^1 \left[f(s,\phi')\, e^{+jk(\bar{\varepsilon}\cdot\hat{\rho})}\right] e^{-jk\rho w'(1-\cos\theta)} \cdot e^{jka\, s \sin\theta\cos(\phi-\phi')}\, s\, ds\, d\phi' \quad . \tag{2.6}$$

Upon examining the integral in (2.6) carefully, we find that the first factor inside the integral is a function of the integration variables alone and the last factor is the Fourier transform kernel written in a polar form. The second factor, viz., $\exp\{-j\kappa\rho w'(1 - \cos\theta)\}$, is a function both of the integration and observation angles, and thus is the factor that requires the special treatment described below.

We define

$$L(s,u,v) = \rho w'(1 - \cos\theta) \tag{2.7a}$$

and

$$L_0 = L(s,u_0,v_0);\ L_a = L(s_a,u,v);\ L_{a0} = L(s_a,u_0,v_0) \tag{2.7b}$$

where s_a is a constant to be determined later and u_0, v_0 are the direction cosines evaluated at $\theta = \theta_0$, $\phi = \phi_0$.

Since $\rho w' = \rho \cos\theta'$ is simply the z-coordinate of the reflector surface, for a symmetric parabola this quantity is a quadratic function of the radial variable s, and is obviously indpendent of the azimuthal variable ϕ'. We make advantageous use of this property of L later. If we now rewrite

$$e^{-jk\rho w'(1-\cos\theta)} = e^{-jL} = e^{-j(L-L_0+L_a-L_{a0})+j(L_0-L_a-L_{a0})}\ , \tag{2.8}$$

we may rearrange (2.6) as

$$E_1(u,v) = \int_0^{2\pi}\int_0^1 \tilde{f} e^{jk(\bar{\varepsilon}\cdot\hat{\rho})+jkas\sin\theta\cos(\phi-\phi')} \cdot e^{-j\Delta} \cdot s\ ds\ d\phi' \tag{2.9a}$$

where

$$E_1 = F(u,v)\ e^{jk2f_a - 2e^{j(L_a-L_{a0})}} \tag{2.9b}$$

$$\tilde{f} = f e^{-jL_0} \tag{2.9c}$$

and

$$\Delta(u,v,u_0,v_0;\ s,s_a) = L - L_0 - L_a + L_{a0}\ . \tag{2.9d}$$

One last step in our manipulation of (2.6) entails the shifting of the origin of the observation coordinates such that it is centered around the beam maximum which is determined by $\bar{\varepsilon}$, the lateral displacement of the feed. This transformation is useful for efficient evaluation of the radiation integral. We choose the new observation variables to be η and α, related to the original direction cosines u and v through the formulas

$$\eta \equiv \sqrt{(u - u_M)^2 + (v - v_M)^2}\ ;\ \alpha \equiv \arctan\left(\frac{v - v_M}{u - u_M}\right)\ ,$$

u_M and v_M being the coordinates of the shifted origin which is here taken to be the beam maximum. Typically u_0, v_0, introduced in (2.7b), are set equal to u_M, v_M, respectively. We can now return to (2.9a) and rewrite the first exponent as

$$k\bar{\varepsilon} \cdot \hat{\rho} + kas \sin\theta \cos(\phi' - \phi) = k\varepsilon_z \cos\theta' + kas[-(\beta_M t_M)\cos(\gamma_M - \phi') + \eta\cos(\alpha - \phi')]$$

where

$$\left.\begin{aligned} \beta_M t_M &\equiv \sqrt{(\beta_{u_M} u_M)^2 + (\beta_{v_M} v_M)^2} \quad , \quad \gamma_M \equiv \arctan\left(\frac{\beta_{v_M} v_M}{\beta_{u_M} u_M}\right) \\ \beta_{u_M} &\equiv -\left(\frac{1}{B_u M} + 1\right) \quad , \quad \beta_{v_M} \equiv -\left(\frac{1}{B_v M} + 1\right) \end{aligned}\right\} \tag{2.10}$$

and where, for a paraboloid,

$$M \equiv 1 + \left(\frac{1}{4\,\frac{f}{D}}\right)^2 s^2 \ .$$

Here we have made use of the relationships

$$\sin\theta' = \frac{s}{2(f/D)\,M} \ ; \ \cos\theta' = \frac{M-2}{M} \ .$$

Lastly, B_u and B_v are the so-called beam deviation factors defined by

$$B_u = \frac{u_M}{u_s}\ (v = 0 \text{ plane}) \quad , \quad B_v = \frac{v_M}{v_s}\ (u = 0 \text{ plane})$$

with $u_s = \frac{\varepsilon_x}{f}$, $v_s = \frac{\varepsilon_y}{f}$. Simple expressions for determining B_u and B_v are given in Appendix I. Using (2.10) in (2.9a) we can rewrite the latter as

$$E_1(u,v) = \int_0^{2\pi}\int_0^1 f_1(s,\phi')\, e^{jkas\eta\cos(\alpha-\phi')}\, e^{-j\Delta}\, s\, ds\, d\phi' \tag{2.11a}$$

with

$$f_1(s,\phi') = f(s,\phi')\, e^{-jL_0}\, e^{jk\varepsilon_z\cos\theta'}\, e^{-jkas\beta_M t_M\cos(\gamma_M-\phi')} \ . \tag{2.11b}$$

The motivation for the manipulations leading up to (2.11) is now given. If we can show that the exponent Δ is small for certain ranges of observation angles to the extent that $\exp[-j\Delta] \approx 1$, we would obtain a Fourier transform form for the radiation integral with an "effective aperture" distribution proportional to f_1.

Referring to the definition of Δ given in (2.9d) and the expressions for the various L's given in (2.7), we immediately see that $\Delta \equiv 0$ at $u = u_0$, i.e., $\theta = \theta_0$ (typically, though not necessarily, the elevation angle θ_M corresponding to the beam maximum). Thus $\exp[-j\Delta]$ is identically equal to 1 for this choice of observation angles. In addition, though not obvious at this point, it turns out that by a suitable choice of s_a, defined in connection with (2.7b), we can make Δ small in the region of integration of (2.9a) from which the dominant contribution of the radiation integral is derived in the wide angle region (typically just a few sidelobes away from the beam maximum) where θ is not close to θ_0. Thus, unusual as it may appear at first sight, what we have accomplished through the manipulations described above is the derivation of an "effective aperture" distribution which is simultaneously valid not only at the beam maximum (as is the ray optical derivation), but at wide angles as well where the ray optical distribution is inaccurate. In fact, numerical results show that only in a small intermediate angular region does the setting of $\exp[-j\Delta] = 1$ in (2.11) introduce any significant errors.

To fill in this gap, we go now to the next step and expand $\exp[-j\Delta]$ in a power series of Δ, obtaining

$$E_1(u,v) = \int_0^{2\pi}\int_0^1 f_1 K\, s\, ds\, d\phi' = j_0 \int_0^{2\pi}\int_0^1 \Delta f_1 K\, s\, ds\, d\phi' - \frac{1}{2}\int_0^{2\pi}\int_0^1 \Delta^2 f_1 K\, s\, ds\, d\phi' \qquad (2.12b)$$

where

$$K = e^{jkas\eta\cos(\alpha-\phi')} = \text{Fourier transform kernel} \qquad (2.12b)$$

in polar form, and Δ was defined in (2.9d). At this point we can compute E_1 by repeatedly Fourier transforming f_1, Δf_1, $\Delta^2 f_1$, etc., which of course

requires an n-fold increase in the number of computations, where n is the number of terms retained in the series. Instead, in the next section, we introduce a series method for computing the first integral in (2.12) which has the unique advantage that the coefficients of the series, once computed, can also be used to evaluate the higher-order terms in (2.12) with very little additional effort or increase in computational time.

In summary, what we have accomplished in expressing the radiation integral in the form of (2.12) is a biconvergent series whose leading term accurately predicts the pattern both in the neighborhood of $\theta = \theta_0$ and at wide angle regions. In addition, because of the special form of Δ, the higher-order terms can be calculated with only a little additional effort beyond that required to evaluate the first term. We substantiate these assertions in the next section where we detail the evaluation of the various Fourier transform integrations in (2.12) using the Jacobi polynomials.

2.3 Evaluation of (2.12) Using Jacobi Polynomials

The first integral in the r.h.s. of (2.12), which has strictly a Fourier transform form, can be evaluated by any number of ways, e.g., using the FFT or expanding f_1 in a series of Bessel functions and evaluating the resulting series of integrals term-by-term in closed form. However, as explained in the last section, our goal is to utilize the results of the first integration for efficiently evaluating the higher-order terms. The expansion functions for f_1 that are uniquely suited for this purpose are the Jacobi polynomials, also referred to as the circle polynomials of Zernicke [4], [5]. The use of the Jacobi polynomial allows one to evaluate the first integral with a speed comparable to the FFT. However, the Jacobi polynomial method has several important advantages over the FFT method, viz., (i) it is better suited for circular apertures; (ii) it can be used to compute the pattern at an arbitrary value of θ, ϕ not restricted by the choice of the FFT-type grid; (iii) it does not suffer from aliasing errors or Gibb's phenomenon; (iv) it is useful for efficiently evaluating higher-order terms whereas the FFT method is not; (v) it has superior numerical accuracy.

The Jacobi polynomial series expansion begins with a two-dimensional Fourier series representation for f_1 in (2.12)

$$f_1(s,\phi') = \sum_{m=0} \sum_{n=0} \left(C_m^n \cos n\phi' + D_m^n \sin n\phi' \right) F_m^n(s) \tag{2.13}$$

$$F_m^n(s) \equiv P_m^n(1 - 2s^2) \equiv 2(n + 2m + 1)\, P_m^{(n,0)}(1 - 2s^2)\, s^n \tag{2.14}$$

where $P_m^{(n,0)}(x)$ are the Jacobi polynomials.

Inserting (2.13) into the first integral in (2.12), henceforth referred to as E_1^0 for convenience, and using the identity

$$\frac{2\pi}{j^n} J_n(z) = \int_0^{2\pi} \cos nu \; e^{-jz\cos u} \, du \quad , \tag{2.15}$$

we get

$$E_1^0(\eta,\alpha) = \sum_n 2\pi j^n \begin{Bmatrix} \cos n\alpha \\ \sin n\alpha \end{Bmatrix} \sum_m \begin{matrix} C_m^n \\ D_m^n \end{matrix} \int_0^1 F_m^n(s)\, J_n(kans)\, s\, ds \tag{2.16}$$

where $\left\{ \right\}$ denotes an upper plus a lower sum. The integral in (2.16) involving the product of Jacobi polynomials, the Bessel function and the weight function can be evaluated in a closed form [6] using the integral relationship

$$a \int_0^1 s^{n+1/2}\, P_m^{(n,0)}(1 - 2s^2)\, J_n(yas)(ys)^{1/2}\, ds = \frac{1}{y^{1/2}} J_{n+2m+1}(ay) \tag{2.17}$$

$$[n > -(m + 1)] \quad .$$

In general we have

$$I_{m,n}(\eta) = \int_0^1 F_m^n(s)\, J_n(ka\eta s)\, s\, ks = \sqrt{2(n + 2m + 1)}\, \frac{J_{n+2m+1}(ka\eta)}{ka\eta} \quad . \quad (2.18)$$

The use of (2.18) in (2.16) permits us to write the final form for the first term of the radiation integral

$$E_1^{(0)}(u,v) = E_1^{(0)}(\eta,\alpha) = 2\pi \sum_{n=0} j^n \begin{Bmatrix} \cos n\alpha \\ \sin n\alpha \end{Bmatrix} \sum_{m=0} 2(n + 2m + 1) \begin{Bmatrix} C_m^n \\ D_m^n \end{Bmatrix} \frac{J_{n+2m+1}(ka\eta)}{(ka\eta)} \quad . \quad (2.19)$$

We note that the radiation integral $E_1^{(0)}$ can be readily calculated at any observation angle u,v [or (η,α)] once the Fourier coefficients C_m^n and D_m^n have been determined. This is in contrast to the direct evaluation of the original integral (2.6) which has to be computed repeatedly for <u>each</u> observation point. We also note from (2.19) that the leading term is the Airy function which is the radiation pattern of a circular aperture with uniform amplitude and phase distribution (except for a linear taper which shifts the beam maximum to u_M, v_M). All of the higher-order terms of the series in (2.19) become zero as $\eta \to 0$ and represent perturbations around the beam maximum.

The expansion coefficients are found in the usual manner after recognizing that the Jacobi polynomials satisfy the orthogonality relationships

$$\int_0^1 P_m^n(1 - 2s^2)\, P_{m'}^n(1 - 2s^2)\, s\, ds = \delta_{m'}^m \quad (2.20)$$

where δ_m^m, is the Kronecker delta. The orthogonality property was one of the criteria employed to select the expansion functions for f_1; the other was the recursion relationship which is used to evaluate the higher-order terms. The integrals to be computed for evaluating the series coefficients are given by

$$\begin{Bmatrix} C_m^n \\ D_m^n \end{Bmatrix} = \frac{\varepsilon_n}{2\pi} \int_0^1 \int_0^{2\pi} f_1(s,\phi') \begin{Bmatrix} \cos n\phi' \\ \sin n\phi' \end{Bmatrix} P_m^n(1 - 2s^2)\, s\, d\phi'\, ds \qquad (2.21)$$

where $\varepsilon_n = 1$ for $n = 0$ and 2 otherwise. An important characteristic of the integrands in (2.21) is that they are far less oscillating than the kernel of the radiation integral (2.6), since the absence of the exponential factor $\exp[jkas \sin\theta \cos(\phi - \phi')]$ makes the kernel of the radiation integral in (2.21) vary much less rapidly compared to the one in (2.6), particularly when $\{ka \sin\theta\}$ is not small.

Before proceeding with the discussion of the steps for the evaluation of the higher-order terms, we examine the leading term E_1^0 in a little more detail with the purpose of showing that this term is useful for the wide angle region as well. This is the biconvergent property alluded to earlier in connection with the series given in (2.12).

In order to explore the wide angles (θ not close to θ_0) behavior of Δ, we refer once again to the definition given in (2.9d) and (2.7) for Δ and the L's, respectively. It is evident that $\Delta \equiv 0$ at $s = s_a$. We now appeal to the well-known result in high-frequency diffraction phenomenon that away from the caustic (beam maximum) the contribution to the secondary radiation comes mainly from the rim of the reflector, described by $s = 1$.

Consequently, if we choose s_a to be equal to 1, we make the exponential factor $e^{-j\Delta}$ close to unity in the neighborhood of the region from where the principal contribution of the radiation integral is derived, in the asymptotic sense, for all observation angles not close to $u = u_0$ ($\theta = \theta_0$). Extensive numerical experiments with different choices of s_a have confirmed that this choice for s_a is the most appropriate one for the symmetric reflector antenna, with or without displaced feeds.

The last topic we discuss in this section is the use of the Jacobi polynomial series for the evaluation of the higher-order terms in (2.12). We begin by explicitly writing L(s,u,v), originally defined in (2.7a). As observed earlier, for a parabola $\rho w'$ is simply the z-coordinate of the reflector surface and this variable is independent of ϕ' and quadratic in s. Explicitly, for a paraboloid of revolution

$$L(s,u,v) = \left\{2\left(\frac{f}{D}\right)\left[-1 + \left(\frac{D}{4f}\right)^2\right]s^2\right\} \cdot \left[\pi\frac{D}{\lambda} - \sqrt{\pi^2\frac{D}{\lambda}^2 - (kau)^2 - (kav)^2}\right]. \tag{2.22}$$

Using the definitions given in (2.7b) and (2.9d), we can write Δ as

$$\Delta(L - L_0) = c\,s^2 - s_a^2\;\; G(u_0,u) \tag{2.23a}$$

where

$$G(u_0,u) \equiv \left\{\sqrt{\left(\frac{\pi D}{\lambda}\right)^2 - (kau_0)^2 - (kav_0)^2} - \sqrt{\left(\frac{\pi D}{\lambda}\right)^2 - (kau)^2 - (kav)^2}\right\},$$

$$c \equiv \frac{1}{8f/D} \;. \tag{2.23b}$$

Substituting (2.23) in (2.12) we obtain

$$E_1(u,v) = \sum_p E_1^{(p)} = E_1^{(0)}(u,v) + E_1^{(1)}(u,v) + E_1^{(2)}(u,v) + \ldots \qquad (2.24)$$

where $E_1^{(0)}$, defined earlier, is the first integral in (2.12), and the higher-order integrals are expressed as

$$E_1^{(1)}(u,v) = jcG \int_0^{2\pi} \int_0^1 \left(s^2 - s_a^2\right) f_1 K \, s \, ds \, d\phi' \qquad (2.25)$$

$$E_1^{(2)}(u,v) = \frac{-(cG)^2}{2} \int_0^{2\pi} \int_0^1 \left(s^2 - s_a^2\right)^2 f_1 K \, s \, ds \, d\phi' \quad . \qquad (2.26)$$

We have already discussed the evaluation of $E_1^{(0)}$ by expanding f_1 in a two-dimensional Fourier series given in (2.13). We now show that by virtue of the recursion relations satisfied by the Jacobi polynomials, the expansion coefficients of the higher-order terms, e.g., $\left(s^2 - s_a^2\right) f_1$ and $\left(s^2 - s_a^2\right)^2 f_1$, etc., can be readily expressed in terms of C_m^n, D_m^n which have presumably been computed already in connection with the evaluation of $E_1^{(0)}$.

To this end we make use of the recursion relationship [6]

$$\left(s^2 - s_a^2\right) P_m^n = a_{mn} P_{m-1}^n + \left(b_{mn} - s_a^2\right) P_m^n + c_{mn} P_{m+1}^n$$

where

$$a_{mn} = -\frac{m(n+m)}{(n+2m)(n+2m+1)}$$

$$b_{mn} = \frac{(m+n)^2}{(2m+n)(n+2m+1)} + \frac{(m+1)^2}{(n+2m+2)(n+2m+1)}$$

$$c_{mn} = -\frac{(m+1)(n+m+1)}{(n+2m+1)(n+2m+2)} \quad , \qquad (2.27)$$

and defining the higher-order expansion coefficients in terms of the integrals

$$\begin{Bmatrix} {}^{p}C_m^n \\ {}^{p}D_m^n \end{Bmatrix} = \frac{\epsilon_n}{2\pi} \int_0^1 \int_0^{2\pi} f_1 \left(s^2 - s_a^2\right)^p \begin{Bmatrix} \cos n\phi' \\ \sin n\phi' \end{Bmatrix} P_m^n(1 - 2s^2)\, s\, ds \qquad (2.28)$$

we can derive

$${}^{p}B_m^n = a_{mn}\, {}^{p-1}B_{m-1}^n + \left(b_{mn} - s_a^2\right) {}^{p-1}B_m^n + c_{mn}\, {}^{p-1}B_{m+1}^n \qquad (2.29)$$

where B represents either C or D. We note from (2.29) that if we retain terms up to the p^{th} order, then the number of coefficients requiring computation is M + p where M is the upper limit of m. Consequently, 2N ($N = n_{max}$) additional series coefficients (N each of C's and D's) are needed for evaluating p integrals of the type $E_1^{(p)}(u,v)$. However, one finds that the higher-order ${}^{p}B_m^n$ coefficients typically decrease very rapidly, allowing truncation to a moderate number of terms and corresponding pairing of computational time.

We summarize this section by noting that we have expressed the radiation integral in (2.12) in terms of a series given in (2.24). We have shown that the first term of the series, viz., $E_1^{(0)}(u,v)$, gives the radiated field for $(u,v) = (u_0,v_0)$ where u_0, v_0 is typically taken to be the beam maximum. The first term also predicts the pattern with good accuracy for θ not too close to θ_0 if we choose $s_a = 1$, since the radiation away from the caustics comes mainly from the rim of the reflector ($s = 1$) and the particular choice of s_a makes Δ small in this region of the "effective aperture." For the intermediate range of observation angles, we can efficiently compute the higher-order integrals in (2.24), i.e., $E_1^{(1)}$, $E_1^{(2)}$, etc., by making advantageous use of the recursion relations of the Jacobi polynomials. In fact, among other reasons, this property of the Jacobi polynomials makes them uniquely suited for our purpose of series expansion.

In the next section we present some numerical results illustrating the application of the theory developed in this paper.

2.4 Steps for Numerical Computations and Illustrative Results

Given the primary pattern of a feed and the parameters of the reflector antenna, the numerical computation of the secondary pattern is carried out using the following steps:

(1) The current distribution $\bar{J}$ on the reflector surface is computed from the knowledge of the feed location $\bar{\varepsilon}$ and its primary pattern using the physical optics approximation.

(2) $f(s,\phi')$ is obtained from (2.4). Note that $\rho \sin\theta' = r$ and $r = as$. The same procedure is repeated for other scalar components of $\bar{J}$ (for details see Appendix II).

(3) Beam deviation factors are computed using the method in Appendix I and u_M, v_M are derived from the coordinates of the phase center of the displaced feed. We also calculate β_M, t_M and v_M appearing in (2.10).

(4) f_1 is derived using (2.11b).

(5) Jacobi polynomials are generated using their recursion relationship [6].

(6) The two-dimensional integration represented in (2.21) is performed to compute C_m^n and D_m^n. The integration may be carried out using any of the standard quadrature routines, e.g., the Gauss quadrature. If a large number of ϕ-coefficients, i.e., n, are required, one may perform the ϕ-integration via the FFT.

(7) The coefficients C_m^n and D_m^n are inserted into the recursion relation (2.29) to generate the higher-order coefficients ${}^pC_m^n$, ${}^pD_m^n$.

(8) $E_1^{(0)}$, $E_1^{(1)}$, $E_1^{(2)}$, etc., are successively computed using these coefficients and Equations (2.19), (2.25) and (2.26) are added up to generate E_1 and subsequently F.

(9) The procedure is repeated for the other components of $\bar{J}$ using the corresponding f.

(10) The vector far-field pattern is constructed by appropriately summing up the various contributions.

We now present a few numerical results to illustrate the convergence of the method. Figure 2 shows the effect of increasing the number of

terms in the Fourier series expansion of f_1, i.e., m_{max} (= M) and n_{max} (= N) for increasing lateral displacement of the feed, e.g., ε_x (or equivalently kau_s). The convergence is seen to be quite rapid even for several beamwidths of scan which is accompanied by a distortion of the secondary pattern.

Figure 3 shows the convergence of the p-series, i.e., (2.24). It is evident that even for a badly distorted pattern only one term of the p-series, i.e., $E_1^{(0)}$, is sufficiently accurate for computing both the amplitude and phase, except in a relatively small, intermediate region $20 < kau < 30$. However, only three terms give sufficiently accurate solutions over the entire range of observation angles.

Before closing this section we remark that unlike the conventional methods the present approach is very well-suited for computing radiation patterns of large reflectors, even several hundred wavelengths in size and, in fact, the relative advantages of the series methods become even more evident when dealing with the large reflector antennas. Since the p-series becomes more rapidly convergent as D/λ is increased, one finds

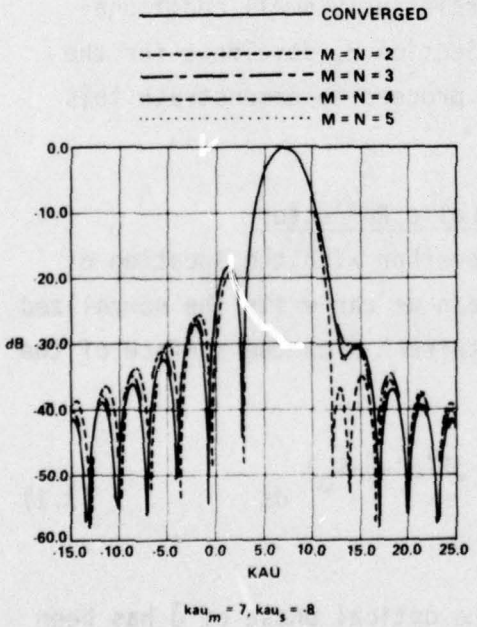

Fig. 2. Series convergence as a function of m and n. $f/D = 0.5$, $D/\lambda = 50$.

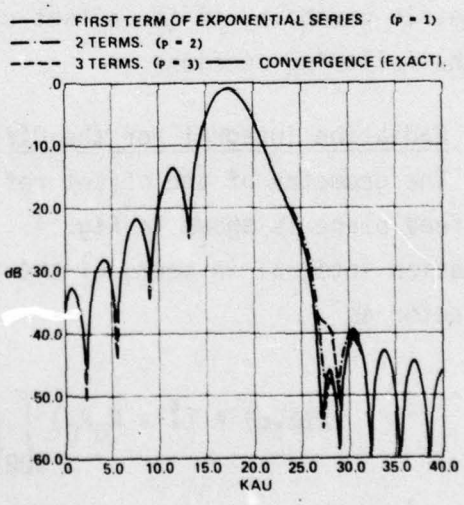

Fig. 3. Convergence of exponential series (2.24).

that the usual numerical problems of storage, loss of accuracy, and astronomical increase of computation time are virtually nonexistent here. Furthermore, $E_1^{(0)}(u,v)$ can be expressed in a scaled form such that the results for the pattern are universal and independent of λ. These added features are quite useful for computation and display of the radiation patterns.

3.0 The Offset Reflector

3.1 Introduction

The offset reflector is finding increasing use in many communication satellite antennas because of its freedom from blockage effects which can affect the performance of a reflector antenna in a deleterious manner. The analysis of offset reflectors is made difficult by the lack of any possible simplifications due to symmetries in the structure. In addition, cross-polarization effects and pattern distortion due to scanning become more important here than in the symmetric case. Thus, accurate but efficient computation of the vector secondary pattern of offset reflectors is highly desired in many applications.

In this work we show that with only a relatively small additional effort one can extend the series method of Section 2, developed for the symmetric parabola, to the offset case. We proceed to demonstrate this in the following sections.

3.2 Radiation Integral for the Offset Parabolic Reflector

The geometry of the offset reflector together with the location of the feed plane is shown in Fig. 4. Once again we can write the normalized radiation integral in terms of the induced current $\bar{J}$ on the surface of the reflector as

$$\bar{E}(\theta,\phi) = (\bar{\bar{I}} - \hat{R}_0\hat{R}_0) \iint_{\text{SURFACE}} \bar{J}\, e^{-jk(\rho' - \bar{\rho}\cdot\hat{R}_0)}\, ds \qquad (3.1)$$

which is identical to (2.1). Recall that the optical phase of $\bar{J}$ has been factored out explicitly relative to an ideal phase center located at $\bar{\varepsilon}$ (see Fig. 4). Also, the integral is defined on the surface A of the

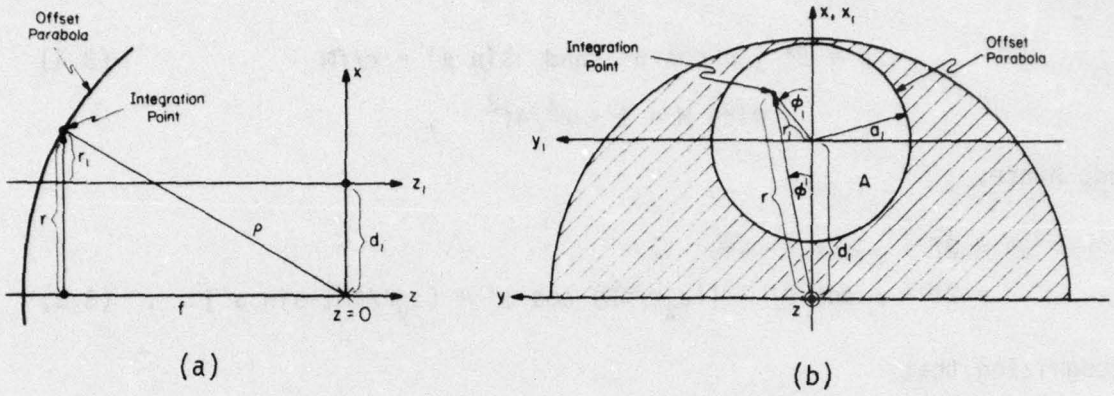

Fig. 4. Geometry of offset parabola.

reflector and not in terms of an approximate, ray optically derived field in the projected aperture.

Introducing a mathematical transformation, we can rewrite the integral in terms of coordinates r, ϕ' of the projected aperture of the parent parabola (see Fig. 4). We get, for a typical scalar component of $\bar{E}$, say, $F(\theta,\phi)$, integrals of the type

$$F(\theta,\phi) = \iint_A f(r,\phi')\, e^{-jk(\rho'-\bar{\rho}\cdot\hat{R}_0)}\, r\, dr\, d\phi' \qquad (3.2)$$

where f is related to the corresponding scalar component of $\bar{J}$ via the Jacobian J of the transformation between the parabolic surface and the projected aperture. The Jacobian J is given by $(1 + r/2f)^{1/2}$.

Using the small displacement approximation, we can write

$$\rho' = \rho - \hat{\rho} \cdot \bar{\varepsilon} \quad . \qquad (3.3)$$

As mentioned earlier, this approximation is easily generalized, if desired, and is not really necessary for our work. However, the small displacement approximation is often used because of its simplicity and because it is sufficiently accurate as long as the feed displacement is not too large.

For a parabola,

$$\rho = 2f + \rho \cos\theta' \quad \text{and} \quad \sin\theta' = r/fM \qquad (3.4)$$
$$\text{with } M = 1 + r^2/4f^2 \quad ,$$

and, hence,

$$\begin{aligned}\rho' &= 2f + \rho\cos\theta' - \hat{\rho}\cdot\bar{\varepsilon} \\ &= 2f + \rho\cos\theta' - [(\varepsilon_x r/fM)\cos\phi' + (\varepsilon_y r/fM)\sin\phi'] \quad . \qquad (3.5)\end{aligned}$$

Recognizing that

$$\begin{aligned}\bar{\rho}\cdot\hat{R}_0 &= \rho\sin\theta'\sin\theta\cos(\phi-\phi') + \rho\cos\theta\cos\theta' \\ &= r\sin\theta\cos(\phi-\phi') + \rho\cos\theta\cos\theta' \quad , \qquad (3.6)\end{aligned}$$

we can rewrite (3.1) as

$$F(\theta,\phi)\, e^{jk2f} = \iint_A \Big\{ f(r,\phi')\, e^{-jk\rho\cos\theta'(1-\cos\theta)}\, e^{jk\varepsilon_z\cos\theta'} \times e^{-jk\beta_1 r(u_s\cos\phi' + v_s\sin\phi')} \times e^{jk\eta r\cos(\alpha-\phi')} \Big\}\, r\, dr\, d\phi' \qquad (3.7)$$

where

$$\beta_1 = \frac{(r/2f)^2 r}{1 + (r/2f)^2} \qquad (3.8)$$

and

$$\alpha = \tan^{-1}\frac{(v + v_s)}{(u + u_s)} \; ; \; \eta = \sqrt{(v + v_s)^2 + (u + u_s)^2} \qquad (3.9)$$

$$\frac{\varepsilon_x}{f} = u_s \; , \quad \frac{\varepsilon_y}{f} = v_s \quad . \qquad (3.10)$$

Examining (3.7), we note the following features of the integrand. In addition to the function f, which is realted to the induced surface current on the reflector, the integral has four exponentials. The first

of these is a function of both the observation angle θ and integration variable $\theta'(r)$. The second and third exponents depend on the integration variables r and ϕ' only. In the second exponent we have deliberately left ε_z to be nonzero, since, in contrast to the symmetric reflector, the plane of displacement of the feed for minimum distortion is not entirely transverse for the offset case. We will soon demonstrate this point when we derive a formula for the optimum feed displacement plane. The third exponent contains u_s and v_s, which define the lateral coordinates of the displaced feed. Finally, the last exponent is the familiar Fourier transform kernel expressed in cylindrical coordinates.

It is desirable for later manipulation to shift the origin of the integration coordinates to the center of the projected aperture. To this end we introduce the transformation of coordinates from (r,ϕ') to (r_1,ϕ_1) system (see Fig. 4) via the equations

$$r \cos \phi' = d_1 + r_1 \cos \phi_1 \tag{3.11a}$$

$$r \sin \phi' = r_1 \sin \phi_1 \tag{3.11b}$$

Writing $F(u,v)\, e^{jh2f} = E_1(u,v)$, we get from (3.7),

$$E_1(u,v)\, e^{-jkd_1\eta\cos\alpha} = \int_0^{a_1} \int_0^{2\pi} \left\{ \tilde{f}(r_1,\phi_1)\, e^{-jkz(r_1,\phi_1)(1-\cos\theta)} \right.$$
$$\times e^{-jk\beta_1 r_1 t_s \cos(\gamma_s-\phi_1)}\, e^{-jk(\beta_1 d_1 u_s - \varepsilon_z \cos\theta')}$$
$$\left. \times e^{jk\eta r_1 \cos(\alpha-\phi_1)} \right\} r_1\, dr_1\, d\phi_1 \tag{3.12}$$

with

$$\tilde{f}(r_1,\phi_1) = f(r,\phi')$$
$$t_s = \sqrt{u_s^2 + v_s^2} \quad ; \quad \tan\gamma_s = u_s/v_s \quad . \tag{3.13}$$

Note also that the r_1 and r are related by

$$r^2 = r_1^2 + d_1^2 + 2r_1 d_1 \cos\phi_1 \quad . \tag{3.14}$$

At this point it is worthwhile to point out some of the similarities and differences between the radiation integrals for the symmetric and offset reflectors. For both of these cases the radiation integral reduces to the Fourier transform form if the first exponent is small, which occurs when $\theta \approx 0$. In the symmetric case the function $z(r_1,\phi_1)$ is independent of the azimuthal coordinate and, in addition, is a quadratic in the radial coordinate. This special property of the z-coordinate of a symmetric parabola allowed us to express the radiation integral in the form of an analytically continuous series whose higher-order coefficients are derivable from those of the corresponding zero-order term via the recursion relationship of the Jacobi polynomials given in the previous section.

It would appear at first sight that this unique and advantageous feature is no longer available for the offset case. Since the function $z(r_1,\phi_1)$ is neither independent of the azimuthal variable ϕ_1, nor is it a quadratic function of r_1. However, we show in Sec. 3.4 that by using a suitable transformation of the observation variables η and α we can still recast (3.12) into a form which has all of the desired characteristics of the symmetric case including the numerical efficiency and ease of computation.

Before discussing this topic, however, we will briefly digress to consider the problem of choosing the optimum scan plane, i.e., ε_z as a function of $(\varepsilon_x,\varepsilon_y)$, for offset reflectors.

3.3 Choice of Optimum Scan Plane

We return to (3.12) and rewrite the third exponent, which contains ε_z, as

$$jk(\beta_1 d_1 u_s - \varepsilon_z \cos\theta') = jk\beta_1[d_1 u_s - 2\varepsilon_z] + jk\varepsilon_z \qquad (3.15)$$

where β_1 was defined in (3.8). This allows us to rewrite (3.12) as

$$\tilde{E}_1(u,v) = E_1(u,v)\, e^{-jk(d_1u_s-\varepsilon_z)-jkd_1u}$$

$$= \int_0^{a_1}\int_0^{2\pi} \Big\{ \tilde{f}(r_1,\phi_1)\, e^{-jkz(r_1,\phi_1)[1-\cos\theta]}$$

$$\times e^{-jk\beta_1 r_1 t_s \cos(\gamma_s-\phi_1)}\, e^{-jk\beta_1[d_1u_s-2\varepsilon_z]}$$

$$\times e^{jk\eta r_1\cos(\alpha-\phi_1)} \Big\}\, r_1\, dr_1\, d\phi_1 \qquad (3.16)$$

where we have used $u = \eta \cos\alpha$. It may be worthwhile to point out that e^{-jkd_1u} represents the phase factor introduced in the expression for the radiation integral due to a shift of the origin from the focus of the parent parabola to the center of the projected aperture.

The criterion we choose for determining $\varepsilon_z(\varepsilon_x,\varepsilon_y)$ is that an optimum choice should minimize the phase error terms represented by the second and third exponential factors in (3.16), exclusive of linear phase tapers which may contribute to beam shift. Explicitly, we deal with the exponent $h(r_1,\phi_1)$

$$h(r_1,\phi_1) = k\beta_1[d_1u_s - 2\varepsilon_z] + k\beta_1[r_1t_s\cos(\gamma_s - \phi_1)] \quad . \qquad (3.17)$$

We note that the first term in the square bracket, i.e., $[d_1u_s - 2\varepsilon_z]$, is independent of r_1 and ϕ_1, whereas the second term contains the factor $r_1t_s\cos(\gamma_s - \phi_1)$, which has a single cosinusoidal variation as a function of the azimuthal angle ϕ_1. Since both of these have a common multiplicative factor $k\beta_1$, one might be tempted to conclude that the minimum distortion due to $h(r_1,\phi_1)$ results when we set

$$2\varepsilon_z = d_1u_s \quad . \qquad (3.18)$$

However, as shown below, the correct choice differs from that given in (3.18) because the behavior of β_1 as a function of (r_1,ϕ_1) can not be ignored. To this end we examine β_1 and express it as

$$\beta_1 = \frac{(r/2f)^2}{1 + (r/2f)^2} = \frac{(r_1/2f)^2 + (d_1/2f)^2 + (r_1/2f)(d_1/2f)\cos\phi_1}{1 + (r_1/2f)^2 + (d_1/2f)^2 + (r_1/2f)(d_1/2f)\cos\phi_1} \tag{3.19}$$

which may be approximated to give

$$\beta_1 \approx \frac{\left[(r_1 + d_1)^2 + 2r_1d_1\cos\phi_1\right]}{\left(4f^2 + r_1^2 + d_1^2\right)} \quad . \tag{3.20}$$

We therefore have

$$\begin{aligned} h(r_1,\phi_1) \approx\ & d_1^2(d_1u_s - 2\varepsilon_z) \\ & + r_1\left[d_1^2t_s\cos(\gamma_s - \phi_1) + 2d_1(d_1u_s - 2\varepsilon_z)\cos\phi_1\right] \\ & + r_1^2\left[(d_1t_s\cos\gamma_s + d_1u_s - 2\varepsilon_z) + d_1t_s\cos(\gamma_s - 2\phi_1)\right] \\ & + r_1^3t_s\cos(\gamma_s - \phi_1) \quad . \end{aligned} \tag{3.21}$$

We note in (3.21) that the parameter ε_z appears only at three places. The first term containing ε_z is a constant in r_1 and merely introduces a constant phase factor in the radiation integral without contributing to distortion. The second term, linear in r_1, also contains ε_z. However, this exponential factor only contains $\cos\phi_1$ and $\sin\phi_1$ types of terms, and hence can be straightforwardly combined with the Fourier transform kernel $-\exp[jk\eta\cos(\gamma_s - \phi_1)]$ to derive the direction of the shifted beam. We show this explicitly in the next section. Meanwhile, we remark here that because of its special form the linear term in r_1 does not introduce any distortion terms either; therefore, we turn our attention to the quadratic term in r_1. It is evident that the first term inside the bracket is independent of ϕ_1, whereas the second term has a cyclical variation along the azimuthal direction. Consequently, the distortion in $h(r_1,\phi_1)$ as a function of ε_z is minimized by enforcing the condition

$$d_1t_s\cos\gamma_s + d_1u_s - 2\varepsilon_z = 0 \tag{3.22a}$$

or

$$\varepsilon_z = (1/2)[d_1 t_s \cos \gamma_s + d_1 u_s] \tag{3.22b}$$

which can be further simplified to give

$$\varepsilon_z = d_1 u_s \tag{3.23}$$

by recognizing that $t_s \cos \gamma_s \approx u_s$. Comparison of (3.23) with (3.18) shows that the two expressions differ by a factor of two. We now show that (3.23) implies that the optimum plane of displacement of the feed is approximately the plane normal to the line OP where P is the point on the surface of the reflector whose projection in the focal plane coincides with the origin ($x = d_1$, $r_1 = 0$) of the projected aperture.

Along this plane ε_{zn} and ε_{xn} satisfy (see Fig. 5)

$$\frac{\varepsilon_{zn}}{\varepsilon_{xn}} = \tan \delta_n = \frac{\sin [\pi - \theta'(d_1)]}{\cos [\pi - \theta'(d_1)]} = \frac{d_1/f_1}{1 - (d_1/2f)^2} \tag{3.24}$$

or

$$\varepsilon_{zn} = \frac{d_1 u_{sn}}{1 - (d_1/2f)^2} \approx d_1 u_{sn} \tag{3.25}$$

for f/D in the range $0.25 \leq (f/D) \leq 1$, since typically $(d_1/2f)^2 < \{1/[8(f/D)]\}^2$ for an offset reflector.

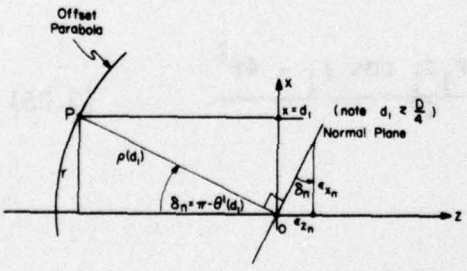

Fig. 5. Geometry of optimum plane for feed displacement.

The result shown in (3.25), though simple, is quite important from a practical point of view. In the past, the choice of the optimum scan plane has been based on experimental trials and a systematic derivation of the equation for the plane has not been available. Before closing this section we add the remark that for the symmetric case, $d_1 = 0$; hence, the optimum scan plane reduces to the focal plane $\varepsilon_z = 0$.

3.4 Series Development of the Radiation Integral

We now return to (3.16) and examine the possibility of developing a series expansion for this radiation integral in the same manner as was done for the symmetric case. We note first of all that in the absence of the first exponential factor $\exp[-jkz(1 - \cos\theta)]$ the integral (3.16) would reduce to a Fourier transform form and could therefore be efficiently evaluated by any number of available methods. Next, we recall that this factor was also present in the symmetric case and that we were able to handle it by using the recursion relations of the Jacobi polynomials because the $z(r,\phi)$ for the symmetric reflector assumed a very special form, viz., quadratic in r and independent of ϕ. The apparent difficulty in using the same procedure for the offset case stems from the fact that z is now a function of both the integration variables r_1 and ϕ_1, and the recursion relationships of the Jacobi polynomials cannot be directly used to efficiently evaluate the coefficients of the Jacobi polynomial series for the higher-order terms of the exponential series derived from the expansion of $\exp[-jkz(1 - \cos\theta)]$. It is extremely fortuitous, however, that certain manipulations of the integrand in (3.16) allow us to retain all of the advantages of the Jacobi polynomial series without any penalty whatsoever. We proceed now to elaborate on this point in the following paragraphs.

As a first step we explicitly write

$$z(r_1,\phi_1) = \rho\cos\theta' = \frac{2f\cos\theta'}{1 - \cos\theta'}$$

$$= \frac{r^2 - 4f^2}{4f} = \frac{r_1^2 + d_1^2 + 2r_1d_1\cos\phi_1 - 4f^2}{4f} \qquad (3.26)$$

for the offset parabola. Thus

$$z(r_1,\phi_1)(1 - \cos\theta) = \frac{d_1^2 - 4f^2}{4f}(1 - \cos\theta) + \frac{r_1d_1}{2f}\cos\phi_1\,(1 - \cos\theta)$$

$$+ \frac{r_1^2}{4f}(1 - \cos\theta) \quad . \qquad (3.27)$$

We now note the following features of the three terms appearing in the r.h.s. of (3.27). The first term is independent of the integration

variables and depends only on the observation angle θ. The second term has a special form in that it is linear in r_1 and has a $\cos \phi_1$ variation. Finally, the last term is quadratic in r_1 and independent of ϕ_1. We will soon make advantageous use of these properties of the first exponent in (3.16).

Turning now to the second exponent in (3.16), we write

$$\begin{aligned}\beta_1 r_1 t_s \cos(\gamma_s - \phi_1) &= \beta_1 r_1 (u_s \cos\phi_1 + v_s \sin\phi_1) \\ &= r_1[(\beta_1 u_s + C_u)\cos\phi_1 + (\beta_1 v_s + C_v)\sin\phi_1] \\ &\quad - r_1[C_u \cos\phi_1 + C_v \sin\phi_1] \qquad (3.28)\end{aligned}$$

where C_u, C_v are constants yet to be specified.

Finally, we rewrite the term $\eta r_1 \cos(\alpha - \phi_1)$ in the last exponent as

$$\begin{aligned}\eta r_1 \cos(\alpha - \phi_1) &= r_1[\eta \cos\alpha \cos\phi_1 + \eta \sin\alpha \sin\phi_1] \\ &= r_1[(u + u_s)\cos\phi_1 + (v + v_s)\sin\phi_1] \quad . \qquad (3.29)\end{aligned}$$

Using (3.27), (3.28) and (3.29), we can now combine certain terms from the various exponents in (3.16) that contain the factors $r_1 \cos\phi_1$ and $r_1 \sin\phi_1$, respectively. We choose to collect

$\underline{r_1 \cos\phi_1 \text{ terms}}$

$$\left\{-\frac{d_1}{2f}(1 - \cos\theta) + C_u + (u + u_s)\right\}$$

$\underline{r_1 \sin\phi_1 \text{ terms}}$

$$\left\{C_v + (v + v_s)\right\}$$

from the various exponents and introduce a new pair of observation variables η_1 and α_1 via the definitions

$$\eta_1 \cos\alpha_1 = -\frac{d_1}{2f}(1 - \cos\theta) + C_u + (u + u_s) \qquad (3.29a)$$

$$\eta_1 \sin\alpha_1 = C_v + (v + v_s) \quad , \qquad (3.29b)$$

hence,

$$r_1[\eta_1 \cos\alpha_1 \cos\phi_1 + \eta_1 \sin\alpha_1 \sin\phi_1] = r_1\eta_1 \cos(\alpha_1 - \phi_1) \quad . \quad (3.30)$$

Using (3.27) through (3.30) in (3.16), we can rewrite

$$a^{-2}\tilde{E}_1(u,v)\, e^{jk\cdot\left[\left(d_1-4f^2\right)/4f\right]\cdot(1-\cos\theta)}\, e^{j(\tilde{L}_a-\tilde{L}_{a0})}$$

$$= E_2(u,v) = \int_0^1\int_0^{2\pi}\left\{f_1(s,\phi_1)\cdot e^{-j\Delta}\, e^{jk\eta_1 s\cos(\alpha_1-\phi_1)}\right\} s\,ds\,d\phi_1 \quad (3.31)$$

where

$$s = ar_1$$

$$f_1 = \tilde{f}\, e^{-jk\beta_1[d_1u_s-2\varepsilon_z]} \times e^{-jka_1s_1[(\beta_1u_s+C_u)\cos\phi_1+(\beta_1v_s+C_v)\sin\phi_1]} \times e^{-j\tilde{L}_0} \quad (3.32)$$

and

$$\Delta = \tilde{L} - \tilde{L}_0 - \tilde{L}_a + \tilde{L}_{a0} \quad (3.33)$$

$$\tilde{L} = \frac{a_1^2s^2}{4f}(1-\cos\theta) = \frac{a_1^2s^2}{4f}\left(1-\sqrt{1-u^2-v^2}\right) \quad (3.34a)$$

$$L_0 = \tilde{L}(s,u_0,v_0) \quad (3.34b)$$

$$\tilde{L}_a = \tilde{L}(s_a,u,v) \quad (3.34c)$$

$$\tilde{L}_{a0} = \tilde{L}(\tilde{s}_a,u_0,v_0) \quad . \quad (3.34d)$$

Comparison of (3.31) with (2.11a), (3.32) with (2.11b), (3.33) with (2.9d) and (3.34) with (2.7) reveals an almost one-to-one correspondence between the equations for the radiation integral for these two cases, provided that the observation coordinates (η,α) for the symmetric case are replaced by (η_1,α_1) for the offset case and certain suitable proportionality factors are introduced in defining E_1 and E_2.

It is evident that the processing of (3.31) can follow exactly the same treatment as (2.11). That is, the function $f_1(s,\phi_1)$ can again be expressed in terms of a two-dimensional Fourier series in s and ϕ_1 in the same manner as in (2.13) and the exponential series for (3.31) be obtained by expanding $\exp[-j\Delta]$ as before. The evaluation of $E_2^{(0)}(u,v)$, as well as

of the higher-order terms of the series, viz., $E_2^{(1)}$, $E_2^{(2)}$, etc., defined in the same manner as in (2.19), (2.24), (2.25) and (2.26), also proceeds in an identical manner with the use of the recursion relation for the Jacobi polynomials for the higher-order terms. In short, all of the advantages of the Jacobi polynomial method of evaluating the radiation integral are maintained in the offset case without any penalty.

Before closing this section, it may be worthwhile to make some comments on the new observation variables η_1, α_1 defined in (3.29). We note first of all that the origin of the observation coordinates, say, u_0, v_0, may be fixed by letting $C_u = (d_1/2f)(1 - \cos\theta_0) - (u_0 + u_s)$ and $C_v = -(v + v_s)$, since $\eta_1(u_0,v_0)$ then becomes identically zero. Typically, though not necessarily, (u_0,v_0) are chosen to coincide with the beam maximum, in which case

$$u_0 = u_m \quad , \quad v_0 = v_m$$

$$C_{um} = (d_1/2f)(1 - \cos\theta_m) - (u_m + u_s) \tag{3.35a}$$

$$C_{vm} = -(v_m + v_s) \tag{3.35b}$$

and we have from (3.29)

$$\eta_1 \cos\alpha_1 = \frac{d_1}{2f}(\cos\theta - \cos\theta_m) + (u - u_m) \tag{3.36a}$$

$$\eta_1 \sin\alpha_1 = v - v_m \tag{3.36b}$$

which are somewhat more convenient to use than (3.29a) and (3.29b).

In order to determine u_m and v_m for a given u_s (= ε_x/f), v_s (= ε_y/f), it is necessary to know the beam deviation factors B_u and B_v. The beam deviation factors for an offset parabola can again be expressed in terms of the primary feed pattern [7].

3.5 Steps for Numerical Computation and Illustrative Results

The steps for numerical computation of the secondary pattern for a given primary pattern of the feed follow pretty much along the lines described in Sec. 2.4.

Some illustrative results of offset pattern computation are shown in Fig. 6. Rapid convergence is achieved (see Fig. 6b) even when the beam

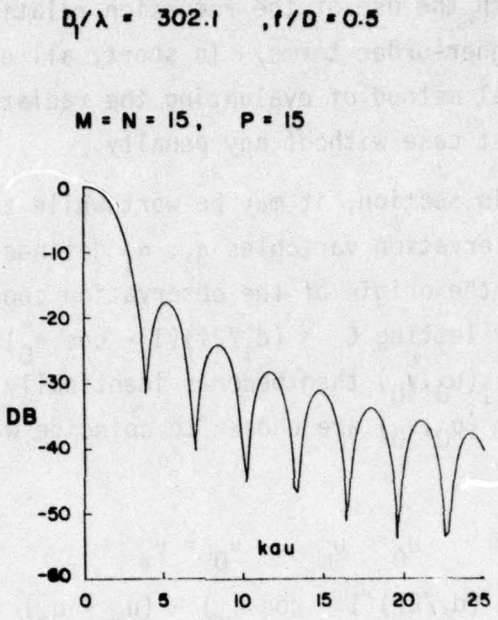

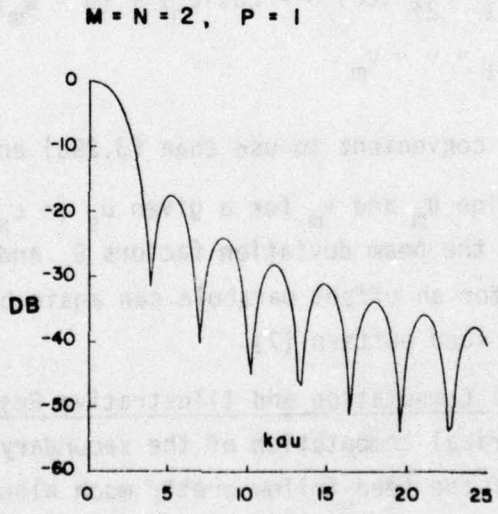

Fig. 6a. Convergence test for offset parabola with focal feed.

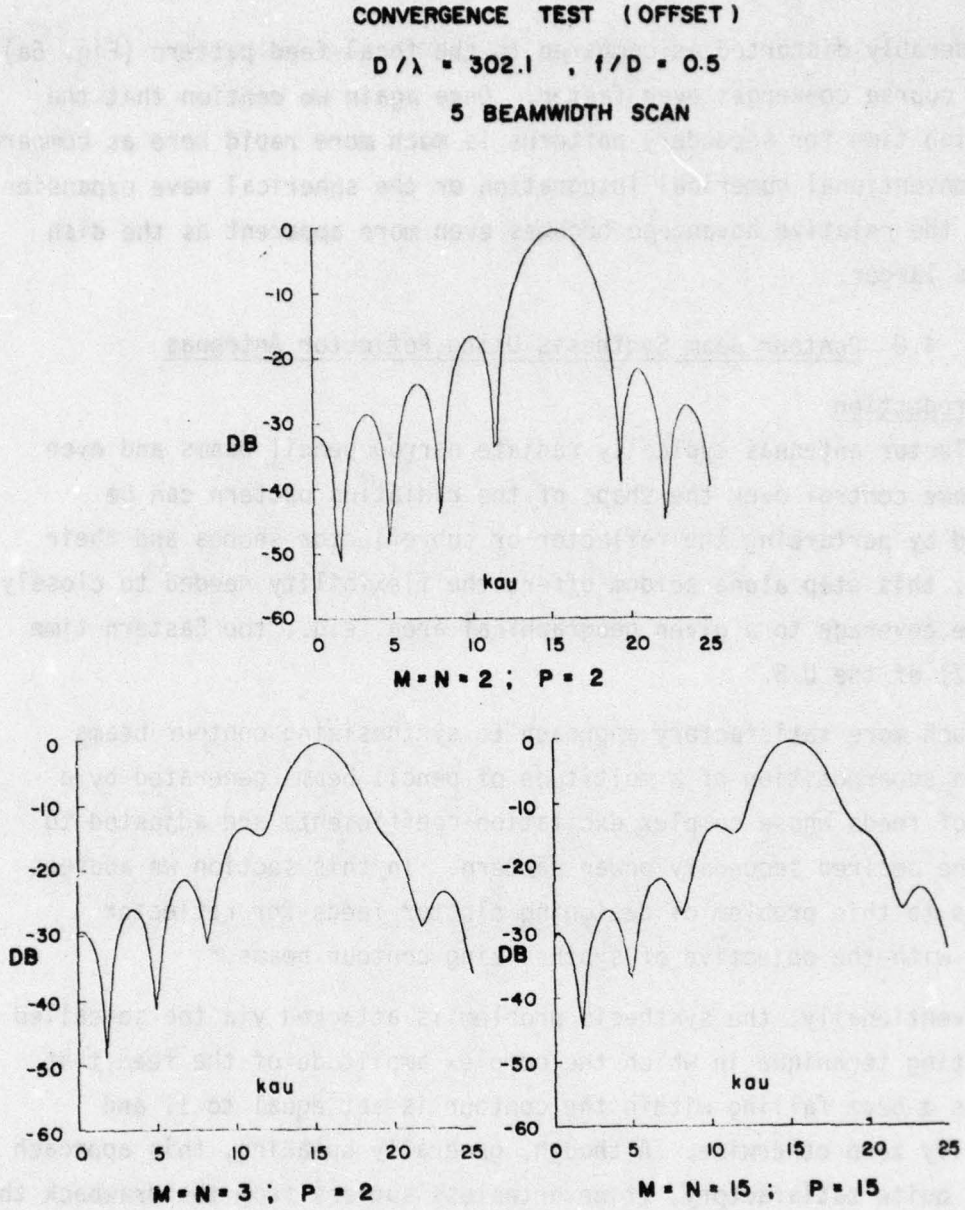

Fig. 6b. Convergence test for offset parabola with displaced feed for 5 BW scan.

is considerably distorted as compared to the focal-feed pattern (Fig. 6a), which of course converges even faster. Once again we mention that the computation time for secondary patterns is much more rapid here as compared to the conventional numerical integration or the spherical wave expansion and that the relative advantage becomes even more apparent as the dish size gets larger.

4.0 Contour Beam Synthesis Using Reflector Antennas

4.1 Introduction

Reflector antennas typically radiate narrow pencil beams and even though some control over the shape of the radiation pattern can be exercised by perturbing the reflector or subreflector shapes and their contours, this step alone seldom offers the flexibility needed to closely match the coverage to a given geographical area, e.g., the Eastern time zone (ETZ) of the U.S.

A much more satisfactory approach to synthesizing contour beams entails a superposition of a multitude of pencil beams generated by a cluster of feeds whose complex excitation coefficients are adjusted to obtain the desired secondary power pattern. In this section we address ourselves to this problem of designing cluster feeds for reflector antennas with the objective of synthesizing contour beams.*

Conventionally, the synthesis problem is attacked via the so-called spotlighting technique in which the complex amplitude of the feed that generates a beam falling within the contour is set equal to 1, and identically zero otherwise. Although, generally speaking, this approach is often quite satisfactory, it nevertheless suffers from the drawback that there is very little control over the slope of the contour, sidelobe level, etc. Perhaps even more important is the fact that the method does not take into account the effect of beam distortion with lateral displacement of the feed, which may be substantial even when the beam scan is only four or five beamwidths.

Neither does the spotlighting method necessarily generate an optimum or "best-fit" solution to the specified contour pattern, which is typically a power pattern, since it attempts to approximate, at best, the specified field pattern while arbitrarily assigning the phase distribution within the

* The material is based on a forthcoming paper [8].

contour to be uniform. Fortunately, however, the spotlighting techniques can still be used to generate results that are very close to the "optimum" one – typically in an extremely efficient manner, providing the constituent beams remain relatively undistorted as these beams are scanned. Obviously, this is not possible to achieve with a single feed unless the reflector is shaped to reduce the scan distortion, a task that is not easily accomplished, and in fact, no systematic means for doing it is available at this time.

Nevertheless, as we show in Section 4.2, a cluster of seven feeds can be synthesized for each scan position such that the beam distortion with lateral displacement is substantially reduced. Superposition of these composite beams using the spotlighting technique can then be employed to synthesize a desired contour beam.

As mentioned earlier, the optimization approach has both the flexibility and capability to handle the general synthesis problem since it can deal directly not only with the specified power pattern, but can also be programmed to achieve some control over the ripple, slope and sidelobes associated with the contour. We discuss this method in Section 4.3 and describe certain algorithms for extracting a numerical solution to the optimization problem. Finally, in Section 4.4, we present some examples of application of both of these methods to the problem of synthesizing the ETZ contour.

4.2 Synthesis of Cluster Feeds to Reduce Pattern Distortion

In this section we discuss two approaches for reducing the distortion in the secondary pattern due to laterally displaced feeds. We begin with the dominant term for the radiation integral, viz., $E^{(0)}(u,v)$, which is given by [see (2.11a)]

$$E_0(u,v) = \int_0^1 s\, ds \int_0^{2\pi} d\phi'\, f_1(s,\phi') \exp[\tfrac{1}{2} jkDsn \cos(\phi' - \alpha)] \quad . \quad (4.1)$$

We restrict ourselves to the case of symmetric reflectors and remind the reader that the derivation of (4.1) was given in Section 2. For convenience, we repeat some of the pertinent definitions:

$$s = r'/a = 2r'/D \tag{4.2a}$$

$$\eta = \left[(u - u_M)^2 + (v - v_M)^2\right]^{1/2} \tag{4.2b}$$

$$\alpha = \tan^{-1}\left[(v - v_M)/(u - u_M)\right] \tag{4.2c}$$

$$u = \sin\theta\cos\phi\ , \quad v = \sin\theta\sin\phi\ . \tag{4.2d}$$

The location of the beam maximum is given by u_M, v_M defined as

$$u = u_M = B_u(\varepsilon/f)\cos\gamma_s \tag{4.3a}$$

$$v = v_M = B_v(\varepsilon/f)\sin\gamma_s \tag{4.3b}$$

where B_u, B_v are the beam deviation factors. The function F_1 is derived from the primary feed pattern, and the location of the feed was defined in (2.11b). It can be rewritten as

$$f_1(s,\phi') = P^*(s)\,Q^*(s,\phi')\,f(s) \tag{4.4}$$

where f(s) is associated with the illumination function of a focal feed [see (2.4)] and is assumed here to be circularly symmetric. The functions P(s) and Q(s) are given by

$$P^*(s) = \exp\left[-j\left\{\tfrac{1}{2}\,k\varepsilon(\varepsilon/f)\,\frac{1+N^2}{1+N^3} - kf(1-N)\left[1 - \sqrt{1-(B_u\varepsilon/f)^2}\right]\right\}\right] \tag{4.5a}$$

$$Q^*(s,\phi') = \exp\{-j[\beta\varepsilon\cos(\phi' - \gamma_M)]\} \tag{4.5b}$$

where

$$N = \left[\frac{s}{4(f/D)}\right]^2 \tag{4.6a}$$

$$\beta = \tfrac{1}{2}\,ks(f/D)^{-1}\left[B_u + (1+N)^{-1}\right] \tag{4.6b}$$

$$\gamma_M = \gamma_s + \pi\ . \tag{4.6c}$$

Note that P and Q are distortion factors introduced by the displacement of the feed, i.e., due to nonzero ε_x and ε_y.

The secondary pattern, which can be calculated using the series expansion method described in Section 2.1, is found to have a distortion for wide angle scan. We have calculated the secondary pattern with the following choice of parameters

$$D = 50\,\lambda\ ,\ f/D = 0.5 \tag{4.7}$$

$$f(s) = (-\cos\theta')^n = \left(\frac{1 - N}{1 + N}\right)^n \tag{4.8}$$

where N was defined in (4.6a) and cos θ' is related to s by the equation appearing underneath (2.10). The exponent n controls the edge taper of the illumination, e.g., n = 2.2538 for a -10 dB taper.

The secondary pattern in dB is plotted in Fig. 7 as a function of kaη. We observe that the beamwidth is approximately 2 × 1.8 in the ka space and that the sidelobes decrease monotonically from the -26 dB level of the first one.

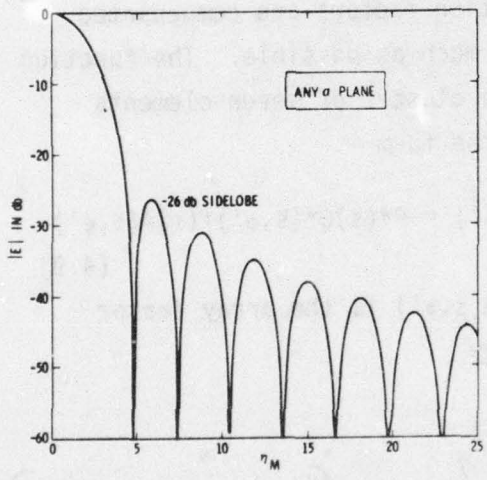

Fig. 7. Secondary pattern of a parabolic reflector due to a focal feed. $D/\lambda = 50$, $f/D = 0.5$ (10 dB edge taper).

In Fig. 8 we have shown the results for the secondary pattern obtained with the feed displaced from the focus to $\varepsilon = 3\lambda$, $\gamma_s = \tan^{-1}(\gamma_s/u_s) = \pi$. We observe from Fig. 8 that the beam becomes quite broad in the scan plane due to phase errors in the aperture. This error also creates higher sidelobes, e.g., -13 dB for the case shown. The effect on the pattern in the plane orthogonal to the displacement of the feed is rather minimal.

We now address ourselves to the problem of compensating for the phase error in the aperture introduced by the displacement of the feed. For this purpose, we consider an array of seven feed elements distributed in a hexagonal lattice shown in Fig. 9. Our problem is to choose the excitation coefficients for the seven feed elements such that the

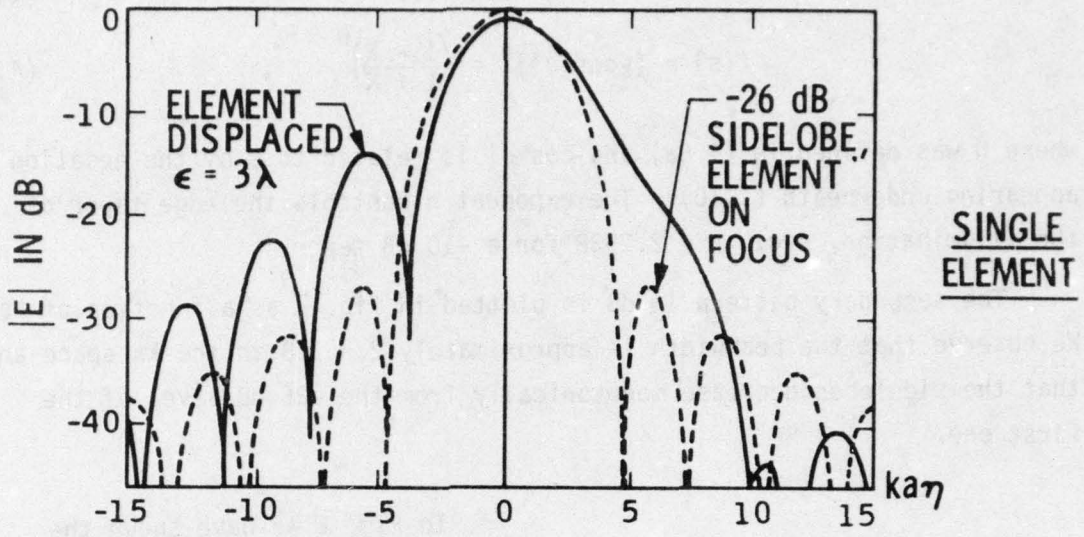

Fig. 8. Secondary pattern distortion due to a displaced feed. Parameters same as in Fig. 7. Note on focus pattern shown in dotted line.

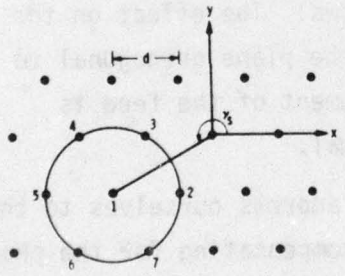

Fig. 9. Feed as a periodic array of equilateral triangular spacing. Elements 1 to 7 form a typical cluster.

distortion factors are compensated for as much as possible. The function for the cluster of seven elements takes the form

$$f_1(s,\phi') = P^*(s)Q^*(s,\phi')f(s)A(s,\phi') \tag{4.9}$$

where $A(s,\phi')$ is the array factor given by

$$A(s,\phi') = 1 + \sum_{m=2}^{7} I_m \exp\left\{ j\kappa d \cos\left[\phi' - (m+1)\frac{\pi}{3}\right]\right\} \tag{4.10a}$$

and where

$$\kappa = k \sin\theta' = ks/\left\{2\left(\frac{f}{D}\right)[1 + N]\right\} . \tag{4.10b}$$

I_m, m = 2,3,4,...,7 in (4a) are the complex excitation coefficients of the ring elements and without loss of generality, we have set the coefficient of the center element equal to 1.

It is evident from (4.9) that to eliminate the distortion from f_1 our goal is to adjust $A(s,\phi')$ such that, ideally,

$$A(s,\phi') = [P^*Q^*]^{-1} \quad , \quad P.Q = 0 < s < 1,\ 0 < \phi' < 2\pi \quad . \tag{4.11}$$

Strictly speaking, it is not possible to achieve the condition enunciated by (4.11) exactly since A has only twelve degrees of freedom. However, we can satisfy (4.11) approximately by matching the leading Fourier coefficients of both sides of this equation. We discuss a method for doing this in the following paragraphs.

The problem of expressing the Fourier coefficients for the expansion of $A(s,\phi')$ is simplified considerably if instead of working directly with the unknown excitation coefficients, we introduce a new set of unknowns $\bar{S}_q$ via the equation

$$I_m = \sum_{q=0}^{5} \bar{S}_q \, e^{jq(m+1)\pi/3} \quad , \quad m = 2,3,4,\ldots,7 \tag{4.12}$$

which is an orthogonal transformation of the I_m. Substituting (4.12) into (4.10) gives

$$A(s,\phi') = 1 + \sum_{q=0}^{5} \bar{S}_q B_q(s,\phi') \tag{4.13a}$$

where

$$B_q(s,\phi') = \sum_{m=2}^{7} \exp\left\{ jkd \cos\left[\phi' - (m+1)\frac{\pi}{3}\right] + jq(m+1)\frac{\pi}{3} \right\} . \tag{4.13b}$$

Making use of the identities

$$e^{jx\cos\theta} = \sum_{m=0}^{\infty} (\varepsilon_m/2)(-i)^m J_m(x)\left[e^{jm\theta} + e^{-jm\theta}\right] \tag{4.14a}$$

$$\sum_{n=0}^{5} \exp j(q+n)\frac{n\pi}{3} = \begin{cases} 6, & \text{if } n+q = 6\ell \\ 0, & \text{otherwise} \end{cases} \tag{4.14b}$$

in (4.13), we get

$$B_q(s,\phi') = 6 \sum_{\ell=-\infty}^{\infty} (j)^{6\ell+q} J_{6\ell+q}(\kappa d)\, e^{j(6\ell+q)\phi'} \qquad (4.15)$$

and eventually the Fourier series for $A(s,\phi')$

$$\begin{aligned} A(s,\phi') = 1 &+ 6\bar{S}_0 \sum_{\ell=-\infty}^{\infty} \varepsilon_\ell (j)^{6\ell} J_{6\ell}(\kappa d) \cos 6\ell\phi' \\ &+ 6 \sum_{\ell=-\infty}^{\infty} (j)^{6\ell+1} J_{6\ell+1}(\kappa d)\left\{\bar{S}_1\, e^{j(6\ell+1)\phi'} + \bar{S}_5\, e^{-j(6\ell+1)\phi'}\right\} \\ &+ 6 \sum_{\ell=-\infty}^{\infty} (j)^{6\ell+2} J_{6\ell+2}(\kappa d)\left\{\bar{S}_2\, e^{j(6\ell+2)\phi'} + \bar{S}_4\, e^{-j(6\ell+2)\phi'}\right\} \\ &+ 6 \sum_{\ell=-\infty}^{\infty} (j)^{6\ell+3} J_{6\ell+3}(\kappa d)\left\{\bar{S}_3\, e^{j(6\ell+3)\phi'}\right\} \quad . \end{aligned}$$

At this point, we note that the product P.Q, which we are attempting to approximately equate to $A(s,\phi')$, is an even function of $(\phi' - \gamma_M)$, whereas the Fourier series given in (4.16) is not. In fact, it turns out that with the limited number of degrees of freedom in our hands, it is not possible to make the function $A(s,\phi')$ even in $(\alpha' - \gamma_M)$ for an arbitrary γ_M. However, it is possible to enforce the condition of evenness to the five Fourier coefficients of $e^{-jp\phi'}$ for $p = 0,\pm1$ and ±2. We can show that this is possible by imposing the two constraints

$$\bar{S}_1 = \bar{S}_5\, e^{-j2\gamma_M} \quad , \quad \bar{S}_2 = \bar{S}_4\, e^{-j4\gamma_M} \qquad (4.17)$$

which reduces the number of unknown coefficients from six to four. Denoting these new unknowns S_q, we relate them to $\bar{S}_q$ via

$$\bar{S}_0 = S_0 \quad , \quad \bar{S}_1 = S_1\, e^{-j\gamma_M} \quad , \quad \bar{S}_2 = S_2\, e^{-j2\gamma_M} \qquad (4.18a)$$

$$\bar{S}_3 = S_3 \cos 3\gamma_M \quad , \quad \bar{S}_4 = S_2\, e^{j2\gamma_M} \quad , \quad \bar{S}_5 = S_1\, e^{j\gamma_M} \quad . \qquad (4.18b)$$

We can also relate the S_q to the original unknowns I_M as follows

$$I_m = S_0 + 2 \sum_{q=1}^{2} S_q \cos q\left[(m + 1)\frac{\pi}{3} - \gamma_M\right] + S_3 \cos 3\left[(m + 1)\frac{\pi}{3} - \gamma_M\right], \quad m = 2,3,\ldots,7 \quad . \tag{4.19}$$

The Fourier series for the array factor becomes

$$\begin{aligned} A(s,\phi') = 1 &+ 6S_0 \sum_{\ell=-\infty}^{\infty} \varepsilon_\ell (j)^{6\ell} J_{6\ell}(\kappa d) \cos 6\ell\phi' \\ &+ 12S_1 \sum_{\ell=-\infty}^{\infty} (j)^{6\ell+1} J_{6\ell+1}(\kappa d) \cos [(6\ell + 1)\phi' - \gamma_M] \\ &+ 12S_2 \sum_{\ell=-\infty}^{\infty} (j)^{6\ell+2} J_{6\ell+2}(\kappa d) \cos [(6\ell + 2)\phi' - 2\gamma_M] \\ &+ 6S_3 \sum_{\ell=-\infty}^{\infty} (j)^{6\ell+3} J_{6\ell+3}(\kappa d) \cos [(6\ell + 3)\phi' - 3\gamma_M] \quad . \end{aligned} \tag{4.20}$$

We note from (4.20) that only the cos $[p(\phi' - \gamma_M)]$ terms appear in the series for p = 0, 1 and 2, thus ensuring the symmetry we were seeking in $A(s,\phi')$ up to these harmonics.

Next we turn to the problem of determining S_q by performing an approximate matching of the array factor A to the distortion factor P . Q. We show that by matching the appropriate Fourier coefficients of A and P . Q we can derive closed form solutions for the coefficients S_q.

Let us first consider the case of $\gamma_M = 0$. The function P . Q may be written in a Fourier series

$$P \cdot Q = P(s) \Sigma\, j^n Q_n(s) \cos n\phi'$$

with

$$Q_n(s) = \varepsilon_n J_n(\beta\varepsilon) \quad . \tag{4.21}$$

From (4.20) we can write

$$A(s,\phi') = \Sigma\, j^n A_n(s) \cos n\phi'$$

with

$$A_0(s) = 1 + 6S_0 J_0(\kappa d) \quad , \quad \text{and} \tag{4.22a}$$

$$A_n(s) = 12S_{|n+6\ell|}\, J_n(\kappa d) \quad , \quad n = 1,2,\ldots \quad . \tag{4.22b}$$

Equating the Fourier coefficients we get

$$A_n(s) = P(s)\, Q_n(s) \quad , \quad \text{for} \quad 0 < s < 1 \quad \text{and} \quad n = 0,1,2,\ldots \quad . \tag{4.23}$$

It is evident, once again, that with only four unknown coefficients it is impossible to satisfy (4.23) for all s. The best we can hope for is a minimization type of solution, e.g., one that minimizes the error* Δ defined by

$$\Delta = \int_0^1 sds \;\; W(s) \sum_{n=0}^{\infty} |A_n(s) - P(s)\, Q_n(s)|^2 \quad . \tag{4.24}$$

In general, we might expect (4.24) to lead to a 4 × 4 matrix equation to be solved for S_q. Fortunately, however, it is possible to diagonalize the resulting equation, enabling one to extract the solution without the need for matrix inversion. To develop this diagonalized form, we first write Δ as

$$\Delta = \sum_{q=0}^{3} \Delta_q \tag{4.25}$$

where

$$\Delta_0 = \int_0^1 (sds)\, W(s) \sum_{n=0}^{\infty} |\delta_n^0 + 6S_0 J_{6n}(\kappa d) - P(s)\, J_{6n}(\beta\varepsilon)|^2 \tag{4.26a}$$

and

$$\Delta_q = \int_0^1 (sds)\, W(s) \sum_{n=-\infty}^{\infty} |6S_q J_{6n+q}(\kappa d) - P(s)\, J_{6n+q}(\beta\varepsilon)|^2 \tag{4.26b}$$

$$q = 1,2,3$$

$$\delta_n^0 = \begin{cases} 1 \;, & n = 0 \\ 0 \;, & n \neq 0 \end{cases} \quad .$$

* Not to be confused with Δ in Sec. 2.

We note that Δ_q depends only on one S, viz., S_q. Thus the individual S_q's can be determined by minimizing the corresponding Δ_q's, one at a time. By requiring

$$\frac{\partial \Delta_q}{\partial S'_q} = 0 \quad , \quad \frac{\partial \Delta_q}{\partial S''_q} = 0 \tag{4.27}$$

where $S_q = S'_q - jS''_q$, we can derive the closed-form solutions

$$S_0 = \frac{\int_0^1 (sds)\, W(s) \sum_{n=0}^{\infty} J_{6n}(\kappa d)\left[P(s)\, J_{6n}(\beta\varepsilon) - \delta_n^0\right]}{6 \int_0^1 sds\, W(s) \sum_{n=0}^{\infty} [J_{6n}(\kappa d)]^2} \quad , \tag{4.28a}$$

$$S_q = \frac{\int_0^1 (sds)\, W(s)\, P(s) \sum_{n=-\infty}^{\infty} \left[J_{6n+q}(\kappa d)\, J_{6n+q}(\beta\varepsilon)\right]}{6 \int_0^1 sds\, W(s) \sum_{n=-\infty}^{\infty} [J_{6n+q}(\kappa d)]^2} \quad , \tag{4.28b}$$

$$q = 1,2,3 \quad .$$

Equation (4.28) represents the solution for S_q we were seeking. We can of course determine the I_M's from (4.19) once S_q are known.

The generalization of the solution to an arbitrary γ_M will now be discussed. First, if $\gamma_M = n\pi/6$, where n is a positive or negative integer, the entire procedure described above for $\gamma_M = 0$ goes right through without change. For $\gamma_M \neq n\pi/6$, it is no longer possible to match all of the ϕ-harmonics but only p = 0, ±1 and ±2 because we do not have a sufficient number of degrees of freedom. Once this fact is accepted, the resulting equations and the solutions for S_q remain unchanged from (4.26).

4.3 Illustrative Results of Cluster and Contour Beam Synthesis

At this point it will be worthwhile to illustrate the synthesis of a single cluster that reduces the distortion in the secondary pattern caused by the lateral displacement of the feed. We refer, once again, to the pattern shown in Fig. 9. We also plot the corresponding "equivalent aperture" distribution [see 2.4] whose Fourier transform gives the secondary pattern under the so-called "small angle approximation"

[see Ref. 3]. We plot this distribution in Fig. 10 for three different azimuthal directions, viz., $\phi' = 0^o$, 90^o (same as -90^o) and 180^o. It is evident that the phase error is quite large in the $\phi' = 0^o$ and 180^o directions. We point out that the error in the phase is the departure from the linear taper which only shifts the direction of the beam. The cluster excitation coefficients that minimize the phase error are found from (4.8) and (4.19) and are given by

$$\left.\begin{aligned} S_0 &= (7.4676 + j\ 0.7144) \times 10^{-2} \\ S_1 &= (9.8688 + j\ 1.2031) \times 10^{-2} \\ S_2 &= (1.0088 + j\ 0.1170) \times 10^{-2} \\ S_3 &= (0.0709 + j\ 0.0099) \times 10^{-2} \end{aligned}\right\} \tag{4.29}$$

and

$$\left.\begin{aligned} I_2 &= -0.1032 - j\ 0.0147 \\ I_3 &= I_7 = -0.0334 - j\ 0.0060 \\ I_4 &= I_6 = 0.1626 + j\ 0.0179 \\ I_5 &= 0.2929 + j\ 0.0336 \end{aligned}\right\} . \tag{4.30}$$

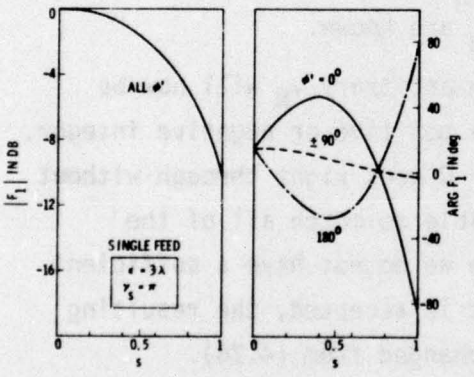

Fig. 10. Equivalent aperture distribution for a single feed whose center element is displaced 3λ in the -x direction.

It is interesting to compare the compensated and uncompensated phase distribution in order to assess the degree of improvement achieved by using a cluster feed as opposed to a single one.

We have plotted the compensated case in Fig. 11 which should be compared with the original phase distribution shown in Fig. 10. The following features may be noted from Fig. 11. The amplitude taper has increased from -10 dB to -14 dB in the $\phi' = 0$ and 180^o plane and to -12 dB in the $\phi' = 90^o$ plane. The improvement in the phase error is notable in the range $0 < s < 0.8$, where the amplitude distribution is relatively significant.

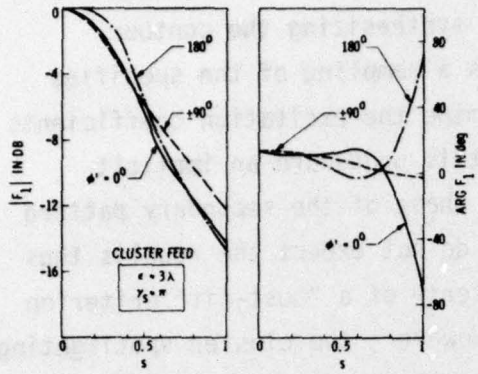

Fig. 11. Equivalent aperture distribution for a cluster feed whose center element is displaced 3λ in the -x direction.

In Fig. 12 we plot the compensated secondary pattern which should be compared to the corresponding uncompensated pattern in Fig. 8. Although the compensated pattern does not by any means reproduce the on-focus feed pattern, it nevertheless reduces the distortion in the secondary pattern quite noticeably.

The sidelobe level in the $\alpha = -180^{o}$ direction is reduced from -13 dB to -17 dB and the shape of the pattern improves in the $\alpha = 0^{o}$ plane. Numerical experiments have been carried out by varying the parameter λ_M and the weight function W(s) of the minimization integral; the basic findings are that the method works as

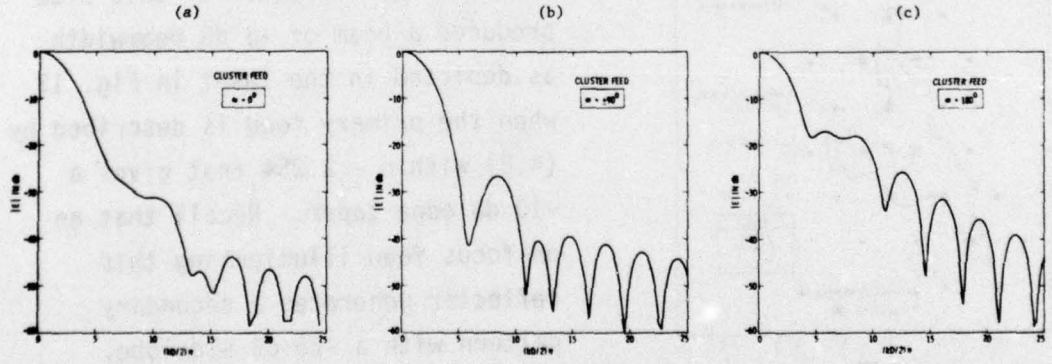

Fig. 12. Compensated secondary pattern with a cluster feed synthesized using equivalent aperture method analytical solution.

well as with an arbitrary λ_M and that varying the weight function has relatively little effect on the results.

Having derived the cluster coefficients, we can use them for synthesizing contour beams in a relatively straightforward manner if we choose to use the spotlighting method for synthesizing the contour coverage. In this method, one merely uses a sampling of the specified contour pattern in the secondary to determine the excitation coefficients of the individual cluster. Note that in this procedure an implicit assumption is made on the behavior of the phase of the secondary pattern which is not specified. Consequently, we do not expect the results thus derived to necessarily be optimum in the sense of a "best-fit" criterion imposed on the specified power pattern. However, the cluster spotlighting method is not only extremely efficient, but the result obtained via the use of this approach often are close to optimum. For this reason the results derived via the spotlighting technique can also serve as good starting points for other iterative techniques.

In Fig. 13 we show the ETZ contour as viewed from a synchronous orbiting satellite located at the equator and at the longitude of 112^{o} W. The scale for this figure is in kau and kav with $D/\lambda = a/2\lambda = 151.05$. A reflector of this size produces a beam of -3 dB beamwidth as depicted in the inset in Fig. 13 when the primary feed is described by (4.8) with n - 2.254 that gives a -10 dB edge taper. Recall that an on-focus feed illuminating this reflector generates a secondary pattern with a -26 dB sidelobe.

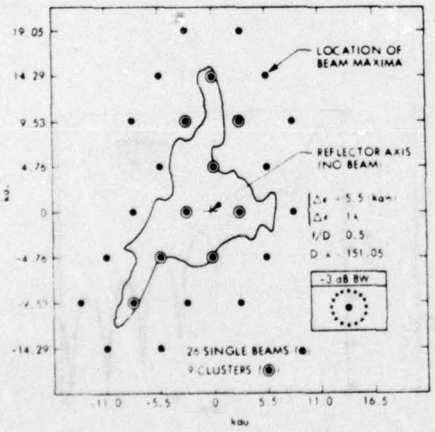

Fig. 13. Eastern Time Zone - synchronous satellite view from equator at 112^{o} W longitude. $D = 151.05\lambda$.

An equilateral triangular lattice of beams is superimposed in Fig. 13 showing the locations of the centers of the spotlighting beams. The separation distance between the feed

elements, which is a design parameter for the system, is chosen to be 1, which produces a -6 dB intersection level between adjacent beams. Such an arrangement assures minimum ripple magnitude when well-formed beams are added in space.

For the size of the reflector chosen for the example, only nine clusters can be positioned such that their main peaks fall inside the contour which spans about 2^{o} as viewed from the synchronous orbit. A total of 26 beams are associated with these nine clusters.

The resulting contour beam realized with the nine-cluster feeds is shown in Fig. 15 and the desired power pattern of the contour is plotted in Fig. 14. The entire design can be carried out using only a few seconds of computer time when the cluster superposition method is used. The field calculation, even at nearly ten thousand or so observation points, can be carried out in a rapid manner using the series approach described in Section 2. It is evident from Fig. 15 that the resolution achieved from the use of a 150 λ diameter dish is not sufficient to accurately follow the contour. Increased resolution can be obtained by

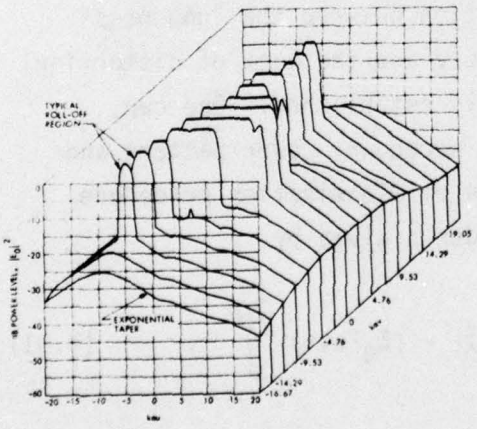

Fig. 14. ETZ objective power pattern function $|E_0(u,v)|^2$.
$ka = \pi D/\lambda = \pi 151.05$.

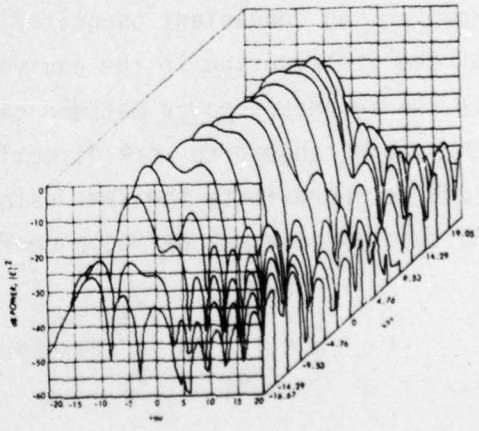

Fig. 15. ETZ contour power pattern function $|E(u,v)|^2$.
$ka = \pi D/\lambda = \pi 151.05$.

using a larger dish; we show in Fig. 16 the results for a 302.1 λ dish. Note that the diagrams have been scaled by the radius a, which is now twice as large compared to the one in the last example. The number of clusters that are accommodated within the contour now increases to 32 and the associated number of single beams is 63. The resolution of the synthesized contour pattern is substantially improved. It should be pointed out, however, that beam distortion puts a severe limit on the maximum achievable resolution and one cannot expect continuous improvement with an increase of reflector size. Although not apparent at first sight, the increase in computation time due to the increase in the number of beams is very little. This is a significant advantage of the cluster synthesis approach developed in this section.

4.4 Gradient Optimization Method

In the last section, we discussed a procedure for synthesizing a contour beam using a spotlighting technique to determine the excitation coefficients of a set of cluster feeds. The tactic employed in this approach was to closely approximate an ideal "equivalent aperture distribution" with that produced by each cluster by varying the relative amplitudes and phases of the individual elements of the cluster. In following this procedure, an implicit assumption is made that a close approximation to the ideal distribution in the "equivalent aperture" will produce a relatively distortionless secondary (field) pattern. However, no convenient quantitative correlation between the "goodness" of the distribution in the equivalent aperture and the lack of distortion in the secondary power pattern can be readily established. One can, therefore, choose to work directly with the secondary power pattern and seek to approximate the same using some type of minimization procedure. To this end one can define a performance index $\bar{\Delta}$ given by

$$\bar{\Delta} = \int_{u_1}^{u_2} du \int_{v_1}^{v_2} dv\, \bar{W}(u,v) \left[|E(u,v)| - |E_0(u,v)| \right]^2 , \qquad (4.31)$$

where $\bar{W}(u,v)$ is a weighting function, $E(u,v)$ is calculated from (4.1) and E_0 is the desired (real) power pattern which can be taken to be the undistorted pattern for a symmetric feed. The region of integration in (4.31) should be taken to be an area in the (u,v) space which is large

enough to cover the range of interest in the secondary pattern space. Any number of available optimization schemes can be employed to minimize $\bar{\Delta}$ and derive the solution for the excitation coefficients I_m's that implicitly appear in (4.31) through the expression for E(u,v). The numerical results for I_m's obtained from an optimal solution of (4.31) are given by

$$\begin{aligned} I_2 &= -0.0816 - j\ 0.0734 \\ I_3 &= I_7 = -0.0250 + j\ 0.0141 \\ I_4 &= I_6 = 0.2034 - j\ 0.0290 \\ I_5 &= 0.2833 - j\ 0.1771 \end{aligned} \tag{4.32}$$

which should be compared with the one derived by working with the "equivalent aperture" method and given in (4.30). The secondary pattern for this choice for I_m's is plotted in Fig. 17. We note that at least for this example the optimal solution is not significantly superior to the secondary pattern derived earlier using the "equivalent aperture" method. However, the computer time required for deriving the optimal solution is considerably higher than that necessary to extract the cluster coefficients using the procedure outlined in Section 4.3. We also mention that the solution for I_m derived from the "equivalent aperture" approach can serve as an excellent initial guess in the gradient optimization program. Finally, it is possible to employ the optimization approach to synthesize the entire contour beam directly, rather than just the constitutent cluster beams. It is not difficult to see, however, that the time involved in deriving an optimal solution directly for the entire contour can be very large and that there is the increased risk of converging to a false minimum.

Although we have not discussed the algorithmic details of optimization procedures, we mention that a number of optimization subroutines are usually available in a typical computer program library. More sophisticated procedures for minimization techniques, such as the minimax procedure, may be found in [9]. An application of this method to the contour beam synthesis problem has been discussed in [10].

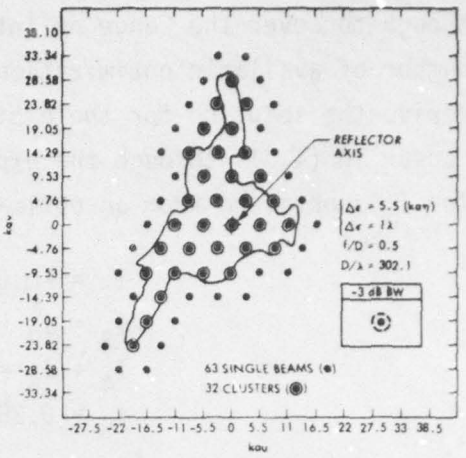

Fig. 16a. Eastern Time Zone — synchronous satellite view from equator at 112° W longitude. D = 302.1λ.

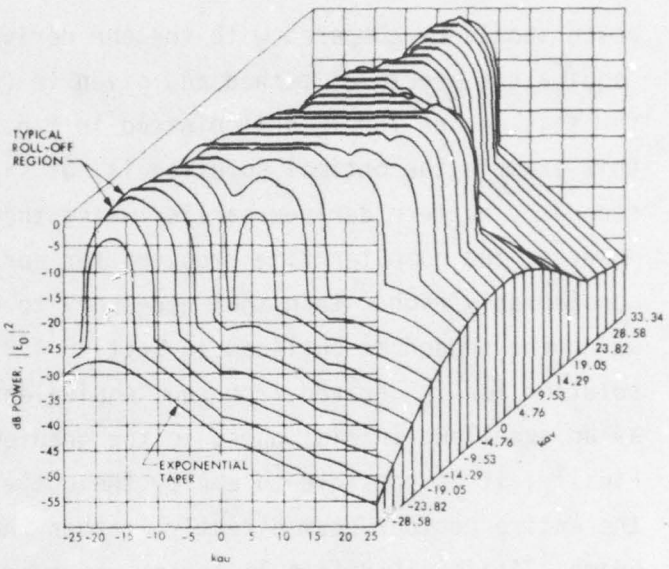

Fig. 16b. ETZ objective power pattern function $|E_0(u,v)|^2$. ka = $\pi D/\lambda = \pi 302.1$.

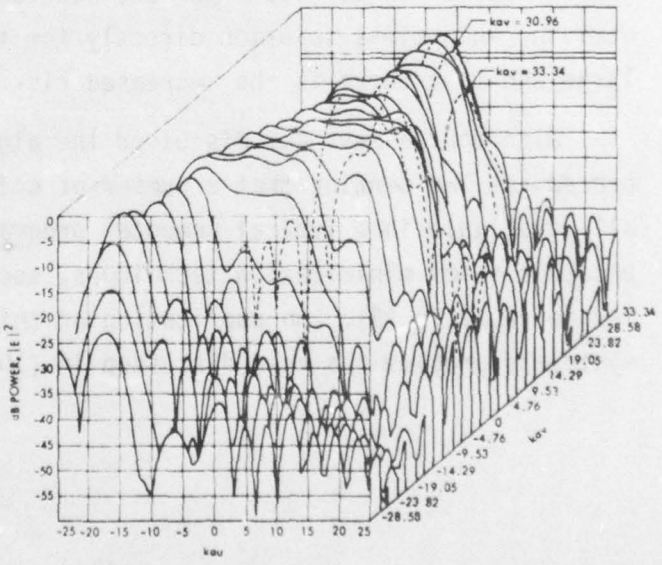

Fig. 16c. ETZ contour power pattern function $|E(u,v)|^2$. ka = $\pi D/\lambda = \pi 302.1$.

(a)

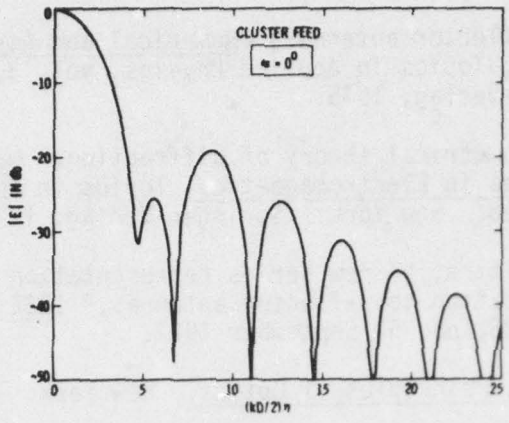

(b)

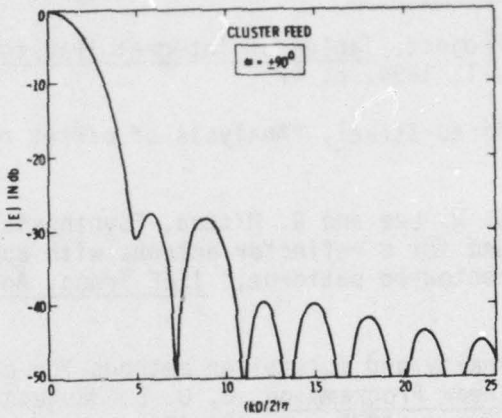

(c)

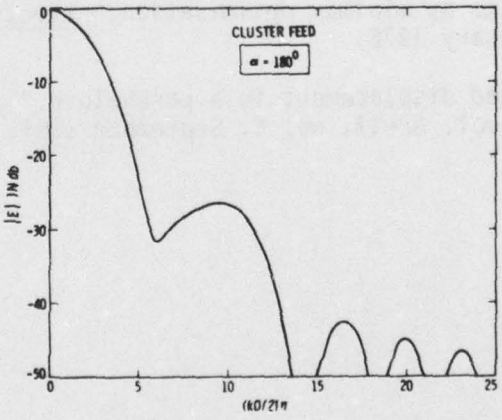

Fig. 17. Compensated secondary pattern of a cluster feed synthesized using the optimization approach.

References

1. W. V. T. Rusch, "Reflector antennas," Numerical and Asymptotic Techniques in Electromagnetics, Topics in Applied Physics, vol. 3, R. Mittra, ed. New York: Springer-Verlag, 1975.

2. R. Kouyoumjian, "Geometrical theory of diffraction," Numerical and Asymptotic Techniques in Electromagnetics, Topics in Applied Physics, vol. 3, R. Mittra, ed. New York: Springer-Verlag, 1975.

3. V. Galindo and R. Mittra, "A new series representation for the radiation integral with application to reflector antennas," IEEE Trans. Antennas Propagat., vol. AP-25, no. 5, September 1977.

4. M. Born and E. Wolf, Principles of Optics. New York: Pergamon Press, 1959, ch. 9.

5. S. Cornbleet, Microwave Optics. New York: Academic Press, 1977.

6. Bateman Manuscript Project, Tables of Integral Transforms, vol. II. New York: McGraw-Hill, 1954, p. 47.

7. R. Mittra and V. Galindo-Israel, "Analysis of offset reflector antennas," (to appear).

8. V. Galindo-Israel, S. W. Lee and R. Mittra, "Synthesis of a laterally displaced cluster feed for a reflector antenna with application to multiple beams and contoured patterns," IEEE Trans. Antennas Propagat. (to appear).

9. D. Bertsekas, "On penalty and multiplier methods for constrained minimization," Nonlinear Programming, 2, O. L. Mangasarian et al., eds. New York: Academic Press, 1975, pp. 165-191.

10. L. W. Pearson and R. Mittra, "Pattern synthesis for antennas with multiple primary beams by minimax optimisation," Electronics Letters, vol. 12, no. 4, February 1976.

11. J. Ruze, "Lateral feed displacement in a paraboloid," IEEE Trans. Antennas Propagat., vol. AP-13, no. 5, September 1965.

Appendix I.

Beam Deviation Factors for Symmetric Reflectors (Parabolic)

The beam deviation factors B_u, B_v are defined by

$$B_u = \left.\frac{u_M}{u_s}\right|_{v=0} \qquad B_v = \left.\frac{v_M}{v_s}\right|_{u=0} \tag{A.1.1}$$

where we recall that u_M and v_M are the direction cosines of the beam maximum and u_s and v_s are given by $u_s = \varepsilon_x/f$ and $v_s = \varepsilon_y/f$. The beam deviation factors are generally independent [11] of the feed displacement, at least when u_s and v_s are not very large. It is also fortuitous that these parameters, which are essentially constants, can be found directly from the primary pattern of the feed centered at the focal point by using

$$B_u = -\frac{\int_0^1 (1 - \cos\theta')[3H_p + E_p]\,\frac{s^3}{M}\,ds}{\int_0^1 (1 - \cos\theta')[3H_p + E_p]\,s^3\,ds} \tag{A.1.2}$$

where E_p and H_p are the E-plane and H-plane patterns of the feed. The other constant B_v can also be derived from (A.1.2) by simply interchanging E_p with H_p.

Appendix II.

A Method for Computing the "Equivalent Aperture" Distribution

We will now briefly outline a method for computing the "equivalent aperture" distribution for a given feed whose primary pattern is known. Let the feed pattern be specified in the (θ',ϕ') coordinate system (Fig. 1) as

$$\vec{E}_{feed} = \frac{e^{-jk\rho}}{\rho} [\hat{\theta}' \; E_{\theta'} + \hat{\phi}' \; E_{\phi'}] \quad . \tag{A.2.1}$$

Assuming that the E- and H-plane patterns of the feed can be smoothly interpolated, we obtain for a nominally $\hat{y}$-polarized feed

$$E_{\theta'} \cong E_p(\theta') \sin \phi' \quad , \quad E_{\phi'} \equiv -H_p(\theta') \cos \phi' \quad , \tag{A.2.2}$$

so that

$$\vec{f}(r,\phi') = - \frac{1}{\eta_0 f} \; (1 - \cos \theta') \left\{ \hat{x} \left[(-H_p + E_p) \sin \phi' \cos \phi' \right] \right.$$
$$\left. + \hat{y} \left[H_p \cos^2 \phi' + E_p \sin^2 \phi' \right] + \hat{z} \left[\operatorname{ctn} \frac{\theta'}{2} \sin \phi' \; E_p \right] \right\} \quad . \tag{A.2.3}$$

Each rectangular component of $\vec{f}$ can now be related to a corresponding component of the surface current.